scientific reports

Check for updates

OPEN

Predicting ground vibration during rock blasting using relevance vector machine improved with dual kernels and metaheuristic algorithms

Yewuhalashet Fissha[1,2]✉, Jitendra Khatti[3]✉, Hajime Ikeda[4], Kamaldeep Singh Grover[3], Narihiro Owada[1], Hisatoshi Toriya[1], Tsuyoshi Adachi[1] & Youhei Kawamura[5]

The ground vibration caused by rock blasting is an extremely hazardous outcome of the blasting operation. Blasting activity has detrimental effects on both the ecology and the human population living in proximity to the area. Evaluating the magnitude of blasting vibrations requires careful evaluation of the peak particle velocity (PPV) as a fundamental and essential parameter for quantifying vibration velocity. Therefore, this study employs models using the relevance vector machine (RVM) approach for predicting the PPV resulting from quarry blasting. This investigation utilized the conventional and optimized RVM models for the first time in ground vibration prediction. This work compares thirty-three RVM models to choose the most efficient performance model. The following conclusions have been mapped from the outcomes of the several analyses. The performance evaluation of each RVM model demonstrates each model achieved a performance of more than 0.85 during the testing phase, there was a strong correlation observed between the actual ground vibrations and the predicted ones. The analysis of performance metrics (RMSE = 21.2999 mm/s, 16.2272 mm/s, R = 0.9175, PI = 1.59, IOA = 0.8239, IOS = 0.2541), score analysis (= 93), REC curve (= 6.85E−03, close to the actual, i.e., 0), curve fitting (= 1.05 close to best fit, i.e., 1), AD test (= 11.607 close to the actual, i.e., 9.790), Wilcoxon test (= 95%), Uncertainty analysis (WCB = 0.0134), and computational cost (= 0.0180) demonstrate that PSO_DRVM model MD29 outperformed better than other RVM models in the testing phase. This study will help mining and civil engineers and blasting experts to select the best kernel function and its hyperparameters in estimating ground vibration during rock blasting project. In the context of the mining and civil industry, the application of this study offers significant potential for enhancing safety protocols and optimizing operational efficiency.

Keywords Blasting, Genetic algorithm, Mining, Particle swarm optimization, PPV, Relevance vector machine

Abbreviations

ANFIS	Adaptive neuro-fuzzy inference system
ANN-BR	Bayesian regularization-based artificial neural network
AOC	Area over the curve
B	Burden
B/De	Burden-to-diameter ratio

[1]Department of Geosciences, Geotechnology, and Materials Engineering for Resources, Graduate School of International Resource Sciences, Akita University, Akita 010-8502, Japan. [2]Department of Mining Engineering, Aksum University, 7080 Aksum, Tigray, Ethiopia. [3]Department of Civil Engineering, Rajasthan Technical University, Kota, Rajasthan, India. [4]Department of Systems, Control and Information Engineering, National Institute of Technology, Asahikawa College, 2-2-1-6 Syunkodai, Asahikawa City, Hokkaido 071-8142, Japan. [5]Faculty of Engineering, Hokkaido University, Kita 8, Nishi 5, Kita-Ku, Sapporo 0608628, Japan. ✉email: yowagaye@gmail.com; jitendrakhatti197@gmail.com

B/S	Burden-to-spacing
BF	Bias factor
Bi	Blastability Index
CAM	Cosine amplitude method
CART	Classification and regression tree
CHIAD	Chi-square automatic interaction detection
D	Hole diameter
df	Degree of freedom
DI	Distance from the blast face
DPR	Delay per row
E	Young's modulus
ELM	Extreme learning machine
f	Rock hardness
F	F state
F Crit	F critical
FA	Firefly algorithm
FIS	Fuzzy inference system
GEP	Gene expression programming
G-LSSVM	Gaussian kernel function-based LSSVM
H/B	Stiffness ratio
HD	Hole depth
HD/B	Hole depth-to-burden ratio
HKM	K-means clustering
HL	Hole length
ICA	Imperialist competitive algorithm
IOA	Index of agreement
IOS	Index of scatter
IQR	Interquartile range
Js	Joint spacing
L-LSSVM	Linear kernel function-based LSSVM
LMI	Legate and McCabe's Index
LSSVM	Least square support vector machine
LSTM	Long short-term memory
MAE	Mean absolute error
MAPE	Mean absolute percentage error
Max.	Maximum
MC	Maximum charge per delay
Min.	Minimum
MS	Means square
MSSD	Mean of the squared successive differences
N	Number of rows
n	Number of drilling holes
N	Number of datapoints
N*	Number of missing datapoints
NMBE	Normalized mean bias error
NS	Nash-Sutcliffe efficiency
PF	Powder factor
PI	Performance index
P-LSSVM	Polynomial kernel function-based LSSVM
PPV	Peak particle velocity
PSO	Particle swarm optimization
Q	Explosive weight
Q_1	First quartile
Q_3	Third quartile
R	Correlation coefficient
R^2	Coefficient of determination
RD	Rock density
REC	Regression error characteristics curve
RF	Random forest
RMR	Rock mass rating
RMSE	Root mean square error
ROC	Receiver operating characteristic curve
RQD	Rock quality designation
RSR	Root mean square error to observation's standard deviation ratio
RVM	Relevance vector machine
S	Spacing
SC	Specific charge
SCA	Sine Cosine Algorithm
SD	Sub-drilling

SD	Scaling distance
SE	Square error
SS	Sum of squares
SSO	Sparrow search optimization
ST	Stemming
StDev	Standard deviation
SVM	Support vector machine
TC	Total charge
TS	Tensile strength
UCS	Uniaxial compressive strength
VAF	Variance accounted for
VIF	Variance inflation factor
Vp	P-wave velocity
WMAPE	Weighted mean absolute percentage error
WOA	Whale optimization algorithm
XGBoost	Extreme gradient boosting

Rock blasting is a frequently used and economically efficient method in the context of mining and civil engineering activities. Blasting is a widely employed technique in mining for obtaining metal and non-metal resources, such as in hard rock mining excavation and quarrying. During quarry operations, the process of blasting entails the systematic drilling of many rows of blast holes, each following to certain requirements for stemming, spacing, burden, sub-drill, face angle, bench height, and hole diameter[1,2].

Different researchers like Fissha et al.[3], underlines approximately 20–30% of the energy generated by the explosion is efficiently used to fragment the rock during blasting. The remaining energy is wasted in various ways, including back break, blasting vibration, fly rock, and air overpressure. The events mentioned have diverse environmental impacts and provide challenges for those living near the area where blasting occurs (Fig. 1). Among these impacts, ground vibration is particularly significant[4–6]. This phenomenon has the potential to

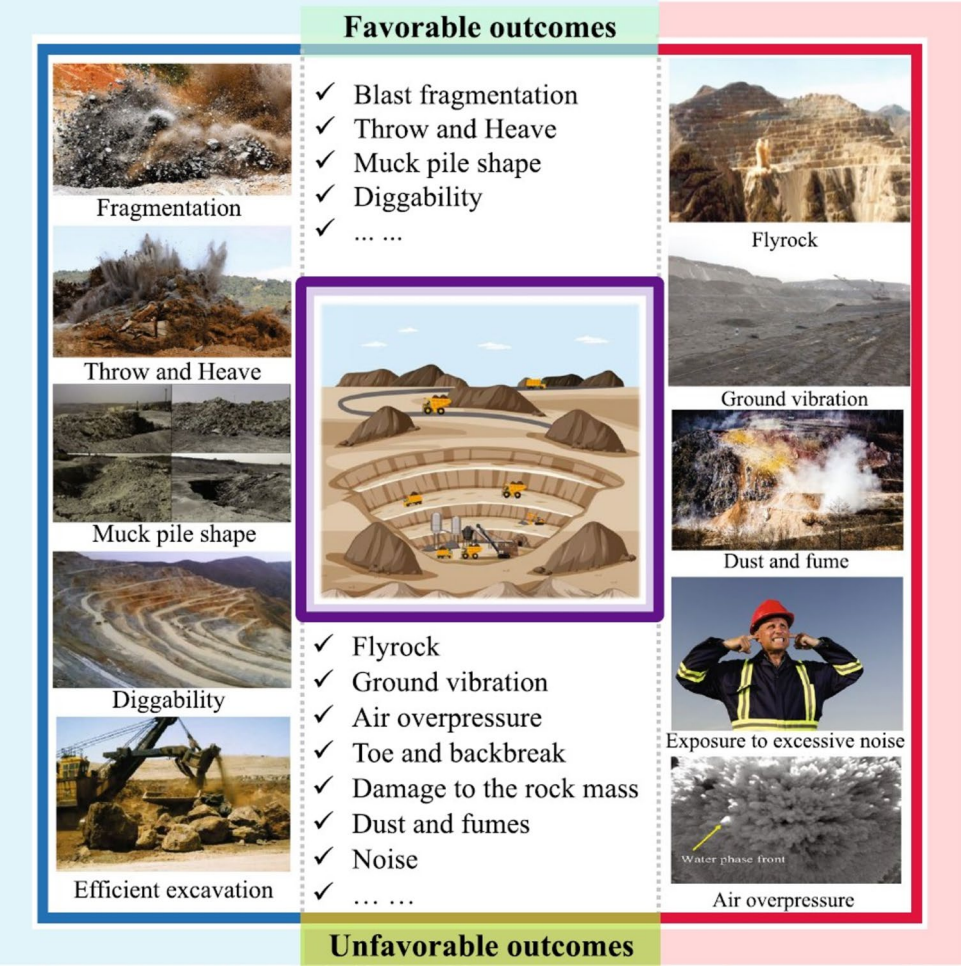

Fig. 1. The favourable and unfavourable outcomes of rock blasting (Source:[9]).

inflict harm on physical constructions and eventually impact the lives and belongings of individuals, especially in cases when the buildings and structures were not specifically engineered to withstand the immense devastation caused by the explosion[7,8]. Explosive-induced ground vibrations have an impact on the development of plants and may result in the loss of forested areas. It also causes ground and slope instabilities, posing a risk to the safety of persons involved in loading, drilling, and subsequent blasting activities. In addition, individuals residing or working in close vicinity to the explosion site may experience physical discomfort as well as stress because of ground vibrations.

Based on Hosseini et al.[10], ground vibration is caused by the energy released during an explosion. The magnitude of the vibration is influenced by several variables, such as the quantity of explosives used, the composition of the rock being exploded, and the distance from the blast source. Lawal et al.[11], state that the strength of the ground vibration caused by explosions is linked to both the factors that can be controlled and those that cannot be controlled during the blasting process. The adjustable parameters for blasting, such as burden, spacing, blast hole depth, hole diameter, stemming type and height, maximum charge weight per delay (W), specific charge, explosive type, detonation velocity (VoD), and powder factor, can be easily adjusted and are meticulously planned according to the current conditions. Hence, it is incumbent upon the blasting engineer to calibrate and formulate these components while devising the blasting methodology.

The uncontrolled variables of the rock include the mechanical and physical properties of the rock, as well as the geological features of the surrounding environment; most uncontrolled factors are contingent upon the rock's inherent creation[12–14].

Mostly the ground vibration movement has a wave-like pattern that propagates in a radial direction away from the blasting source[11,15]. Figure 2 shows the movement of waves during blasting vibration. This wave motion has similarity to the circular ripples that propagate outward when an object hits into a body of water and comes into contact. The PPV is the main parameter utilised to assess the magnitude of ground vibration resulting from blasting activities. PPV represents the velocity of the primary particles in terms of their transverse (T), vertical (V), and longitudinal (L) velocity.

Several scientists have established empirical formulae to anticipate the amplitude of blast-induced ground vibration coming from blasting operations. One of the earliest and most important equations to estimate PPV was developed by the USBM, Duvall, and Fogleson[17–19]. After many years, numerous academics produced adjustments to the USBM formula, considering the scaled distance and MC. The mathematical formulation of these techniques is found in Table 1. However, the precision of the predictive model, the assessment of the complex nature of the rock mass conditions and input data parameters, and other factors contribute to the increased difficulty and time required for predicting and estimating blasting vibration. Hence, empirical models are inadequate due to the constraints imposed by their empirical formulations.

With the advent of digitalization, numerous researchers have begun employing artificial intelligence techniques such as machine learning, and deep learning methodologies to forecast blast-induced ground vibrations. The study by Hosseini et al.[10], aims to analyse advanced deep learning, machine learning, and hybrid learning

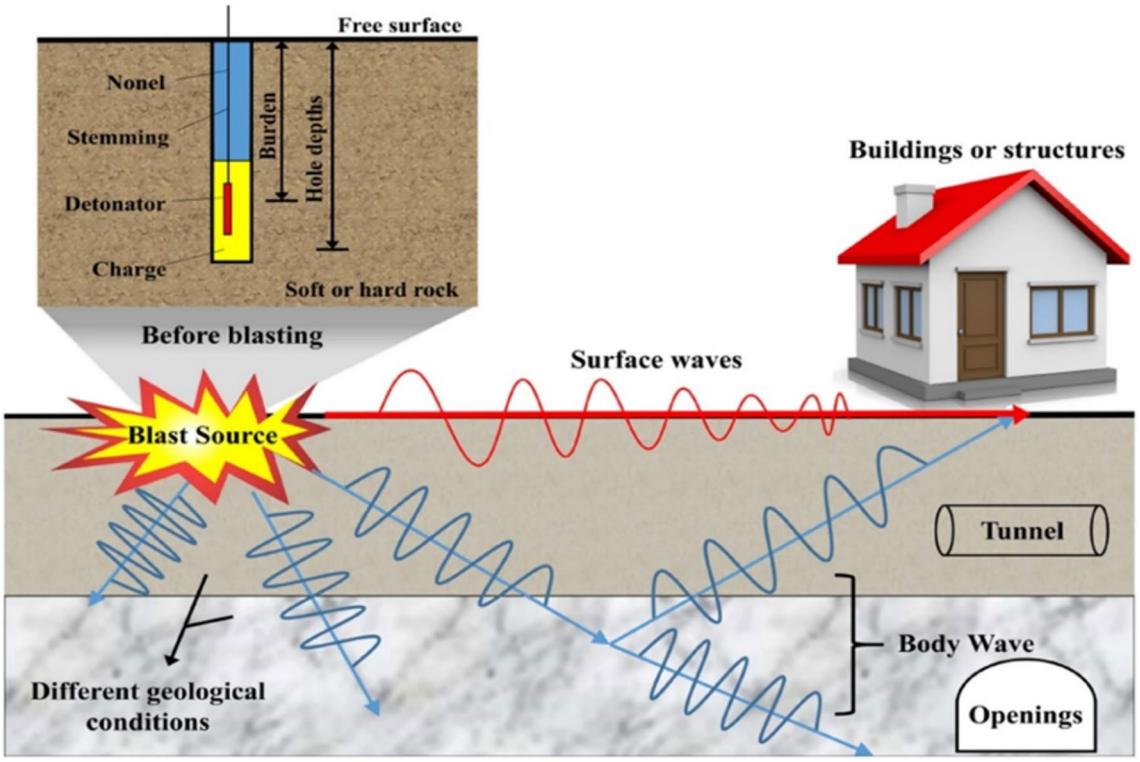

Fig. 2. Propagation of ground vibration wave during rock blasting (Source:[16]).

Name of empirical formula	Empirical equations
Duvall and Fogleson (USBM)	$PPV = K\left(\frac{D}{Q^{1/2}}\right)^{-b}$
Ambraseys and Hendron	$PPV = K\left(\frac{D}{Q^{1/3}}\right)^{-b}$
Langefors and Kihlstrom	$PPV = K\left(\frac{D^{1/2}}{Q^{3/4}}\right)^{b}$
Indian standards	$PPV = K\left(\frac{D}{Q^{2/3}}\right)^{b}$

Table 1. Empirical equations applicable for the prediction of blast-induced vibrations. D is the distance from the blasting face to the monitoring station (m), PPV is the peak particle velocity (mm/s), and Q is the maximum instantaneous charge (kg), whereas k and b are the site constants; each site has its site constants (k and b).

methods to provide an appropriate computational model for quantifying ground vibrations in mining blasting activities. The ANN, LSTM, ET, LSSVM, DT, SVM, GPR, and MLR models are utilised with a dataset consisting of 162 data points. The new black hole-optimized LSTM model has been utilised for the initial time to predict ground vibrations resulting from blasting. 15 performance metrics have been devised to precisely evaluate the predicting capabilities of different ML models. Table 2 presents a brief overview of the most recent research on utilising machine learning to predict ground vibrations.

Novelty of the research

The present investigation has the following novelty.

- The present study analyses and employs the capabilities of RVM models in assessing and predicting ground vibration for the first time.
- This study compares the conventional RVM models configured by Laplacian, linear, Gaussian, exponential, sigmoid, and polynomial kernels. In addition, these models have been enhanced by the application of both genetic and particle swarm optimisation algorithms. Also, the comparison of conventional, genetic, and particle swarm-optimized single kernel-based RVM models reveals the impact of optimization on the accuracy and performance of RVM models.

Authors	AI technique	Number of datapoints	Details of input variables		R^2 test
			Variables	No.	
Nguyen et al.[20]	SSO-ELM	216	B/S, DI, ST, MC, PF, HD, RQD, N, SD	9	0.91
Zhang et al.[21]	**RF**, CART, CHAID	102	DI, MC	2	0.94
Zhou et al.[22]	RF	102	DI, MC, PF, B, S, HD	6	0.93
Huang et al.[23]	FA-ANN	88	DI, MC, B, S, N	5	0.91
Zhou et al.[24]	GEP-MC	102	B/S, DI, ST, MC, PF, HD	6	0.91
Nguyen et al.[25]	SVR-GA	125	DI, MC	2	0.99
Nguyen et al.[26]	HKM-CA	136	DI, MC	2	0.99
Armaghani et al.[27]	ICA	73	B, S, ST, D, HD, PF, MC, DI	8	0.95
Hasanipanah et al.[28]	CART	86	DI, MC	2	0.95
Ghoraba et al.[29]	ANN, **ANFIS**	115	DI, MC	2	0.95
Shirani Faradonbeh et al.[30]	GEP	102	DI, MC	2	0.88
Hajihassani et al.[31]	ICA-ANN	95	MC, DI, TC	3	0.98
Hajihassani et al.[32]	PSO-ANN	88	BS, ST, PF, MC, DI, Vp, E	7	0.89
Hasanipanah et al.[33]	SVM	80	RD, E, UCS, TS, Js, B, S, HD/B, SC, ST, DPR, DI	12	0.96
Armaghani et al.[34]	ANFIS	109	BS, MC, HD, ST, SD, DI, PF, RQD	8	0.97
Armaghani et al.[35]	PSO-ANN	44	B, S, ST, N, MC, DI	6	0.94
Mohamadnejad et al.[36]	**SVM**, ANN	37	DI, MC	2	0.89
Monjezi et al.[37]	ANN	182	CD, DI, ST, HD	4	0.95
Mohamed[38]	**ANN**, FIS	162	DI, MC	2	0.94
Fişne et al.[39]	FIS	33	DI, MC	2	0.92
Iphar et al.[40]	ANFIS	42	DI, CD	2	0.99

Table 2. Provides an overview of several machine learning models discussed in the literature review. The bold letters represent the most optimal soft computing model in the research.

- This investigation employs dual kernel (k1 + k2) RVM models (k1 kernel is selected from the comparison of non-optimized single kernel RVM models). Thus, this research employs five dual kernels based RVM models and optimizes them using each genetic and particle swarm optimization algorithm.
- Fifteen metrics, WI, LMI, RSR, MBE, NMBE, NS, BF, PI, VAF, MAPE, R, MAE, WMAPE, RMSE, IOS, IOA, and a20, evaluate the performance and precision of each model and showcase the dependability of the models.

Research significance

This study addresses the significant issue of blast-induced ground vibrations in sectors like mining and construction. Conventional models see (Table 1) often fall short due to oversimplified approaches. By employing relevance vector machines (RVM), this research offers a novel method to precisely analyse vibrations, considering complex relationships and uncertainties. This not only advances academic understanding but also provides practical insights for risk assessment and mitigation. The flexibility of the proposed model makes it valuable for various blasting scenarios, benefiting engineers, policymakers, and researchers in addressing environmental and structural impacts.

The rest of the paper is organized as follows: the research methodology of this study is provided in "Research methodology", and details regarding the datasets and preprocessing, data analysis, and developing soft computing approaches are included in "Data analysis and soft computing approaches". Section "Results and discussion" outlines the results and discussions of the RVM model predictions and the results of the different statistical analyses. The key conclusions and remarks from the research and their implications are presented in "Conclusion and summary".

Research methodology

This study presents an optimised performance model for accurately predicting ground vibration caused by blasting using several RVM models. Two hundred datasets have been gathered from published work by Hammed et al.[41] to test, train, and validate the RVM models. The data is collected from ten quarry sites in Nigeria. The dataset consists of different variables such as charge weight (*W*) in Kg, monitoring distance (*D*) in meters, scaled distance (*SD*) in m/kg½, and peak particle velocity (*PPV*) in mm/s. In this study, the PPV is the target output of the investigation hence we consider one vector sum PPV only because the data set from the literature consists of three different PPVs based on their vectorial direction such as longitudinal, vertical, and transverse. PPV by default it is a vector quantity so, it follows vector sum. The data set of this study is summarised in Table 3, as follows.

Using the data proportionality method, the testing, validation, and training databases have been created by selecting 20, 20, and 160 data points arbitrarily. In this study, we developed thirty-three RVM models. The conventional single kernel based SRVM models were developed using linear, polynomial, Gaussian, sigmoid, exponential, and Laplacian kernel functions. Therefore, these SRVM models were optimized by each GA and PSO algorithm. Conversely, to determine the kernel 1 (k1), the effectiveness of conventional SRVM models was evaluated. After finding k1, the different combinations of kernels were prepared. In this research, the Gaussian kernel based conventional SRVM model achieved higher performance. Hence, the following combinations were prepared to develop the dual kernel based DRVM model: (1) Gaussian + linear, (2) Gaussian + exponential, (3) Gaussian + sigmoid, (4) Gaussian + Laplacian, and (5) Gaussian + polynomial. Thus, five conventional DRVM models were developed, similarly the five DRVM models were optimized each by PSO and GA algorithms are compared and analysed to introduce an optimal performance model for predicting the ground vibration during blasting. To compute the performance of each model, the, *LMI, WI, NMBE, RSR, BF, PI, NS, MBE, WMAPE, VAF, MAPE, RMSE, R, MAE, IOS, IOA, and a20* statistical metrics were implemented. These statistical metrics have been compared for each case, i.e., *SRVM, SRVM_GA, SRVM_PSO, DRVM, DRVM_GA, and DRVM_PSO*, and determined six better-performing models. In addition, the score analysis has been performed and compared for each model. Furthermore, the predictive abilities of the six top-performing models have been examined by visualising the regression error characteristics (REC) curve. Uncertainty analysis, Wilcoxon test, and Anderson–Darling (AD) test were conducted on the better-performing models to determine the ideal performance model for predicting ground vibration in blasting. Additionally, the optimum performance model has undergone calculations for curve fitting, generalizability, and internal validation. After conducting several analysis and experiments, this study presents an optimum RVM model for precisely predicting ground vibration in rock blasting. Figure 3 illustrates the comprehensive flow of the research approach used in this study.

Software support

MATLAB R2020a: for developing soft computing models, evaluation, analysis, and prediction. Origin Lab 2022b: for graphical presentations and data analysis, and Minitab Statistical Software: for statistical analysis.

Data analysis and soft computing approaches

Data analysis

The authors investigated a dataset collected from Hammed et al.[41], to develop accurate predictive models for the PPV. The dataset consisted of 200 test results for the PPV induced from the quarry blasting in Nigeria. The data analysis section is done using Origin Pro 2024 software. Table 4 reveals the summary of the database's descriptive statistics. It also contained many possible input factors that were believed to have an impact on the PPV. Figure 4 provides further clarification on the distribution of each variable using a frequency histogram plot in navy blue (left) and ridgeline plots in orange (right). This study utilizes both frequency histograms and ridgeline plots to verify the normal distribution of the dataset for each variable. Based on this analysis, each variable shows a normal distribution. The visual representation of the data in this figure is advantageous for identifying any possible

Data monitoring points	Distance (m)	Charge per delay (kg)	Scaled distance (m/kg½)	PPV (mm/s)	Peak particle velocity (mm/s)		
					Vertical PPV (mm/s)	Longitudinal PPV (mm/s)	Transvers PPV (mm/s)
1	300	1850	6.97	189.46	110.5	109.45	108.2
2	350	1850	8.14	149.16	86.25	85.95	86.15
3	400	1875	9.24	122.17	70.45	71.25	69.65
4	450	1950	10.2	104.3	60.2	60.35	60.1
5	500	1950	11.32	87.1	50.9	50.2	49.75
6	550	1950	12.46	75.46	43.7	43.85	43.15
7	600	1950	13.59	68.68	39.5	40.5	38.95
8	650	1875	15.01	56.32	32.35	32.75	32.45
9	700	1875	16.17	48.74	28.8	27.5	28.1
10	750	1875	17.32	43.62	25.75	24.95	24.85
11	800	1912.5	18.29	40.48	23.6	22.65	23.85
12	850	1912.5	19.44	36.69	21.45	21.15	20.95
13	900	1912.5	20.58	33.81	19.55	19.15	19.85
14	950	1900	21.79	31.23	17.85	18.95	17.25
15	1000	1875	23.09	28.21	16.25	16.85	15.75
16	1050	2950	19.33	36.7	21.65	20.75	21.15
17	1100	1800	25.93	22.98	13.5	13.05	13.25
18	1150	2750	21.93	30.99	17.65	18.75	17.25
19	1200	2150	25.88	23.42	13.55	13.05	13.95
20	1250	2050	27.61	21.08	12.2	11.75	12.55
21	300	1450	7.88	156.95	90.85	90.75	90.25
22	350	1450	9.19	100.94	71.05	71.3	70.95
23	400	1400	10.69	96.18	55.75	55.75	55.08
24	450	1450	11.82	82.13	47.5	47.4	47.35
25	500	1400	13.36	67.64	39.05	39.15	38.95
26	550	1500	14.2	60.63	35.45	35.55	35.75
27	600	1200	17.32	45.63	25.7	25.85	27.45
28	650	1850	15.11	55.48	32.05	32	32.05
29	700	1850	16.27	49.19	28.4	28.45	28.35
30	750	950	24.33	25.81	14.95	14.9	14.85
31	800	1350	21.77	30.8	17.8	17.7	17.85
32	850	1250	24.04	26.33	15.25	15.2	15.15
33	900	1250	25.46	23.51	13.95	13.8	12.95
34	950	1500	24.53	25.32	14.75	14.85	14.25
35	1000	1500	25.82	23.3	13.5	13.25	13.35
36	1050	1750	25.1	24.39	14.25	13.95	14.05
37	1100	2350	22.69	28.32	16.75	16.05	16.25
38	1150	1350	31.3	17.26	10	9.85	10.05
39	1200	1450	31.51	16.75	9.9	9.85	9.25
40	1250	2755	23.81	26.36	15.5	15.2	14.95
41	300	1650	7.39	174.16	100.75	101.05	99.85
42	350	1550	8.89	128.35	74.9	73.45	73.95
43	400	1355	10.89	94.17	54.3	54.95	53.85
44	450	1555	11.22	86.63	50.25	49.75	50.05
45	500	1850	11.62	83.8	48.75	48.35	48.05
46	550	1900	12.62	62.24	35.95	36.15	36.95
47	600	1400	16.03	50.67	29.15	29.75	28.85
48	650	1100	19.6	36.17	21.15	20.55	20.95
49	700	1250	19.8	34.77	20.8	21.05	20.1
50	750	1500	19.3	36.41	21.55	20.45	21.05
51	800	1800	18.86	38.42	22.45	22.1	21.95
52	850	1950	19.25	36.85	21.75	20.65	20.05
53	900	1250	25.46	23.42	13.9	13.1	13.55
54	950	1250	26.87	21.25	12.75	11.95	12.1
55	1000	1200	28.88	18.62	10.75	11.05	10.45

Continued

Data monitoring points	Distance (m)	Charge per delay (kg)	Scaled distance (m/kg½)	PPV (mm/s)	Peak particle velocity (mm/s)		
					Vertical PPV (mm/s)	Longitudinal PPV (mm/s)	Transvers PPV (mm/s)
56	1050	1950	23.78	26.58	15.5	14.55	15.95
57	1100	1800	25.93	22.73	13.05	13.55	12.75
58	1150	1800	27.11	21.17	12.55	11.85	12.25
59	1200	1800	28.28	19.44	11.75	10.65	11.25
60	1250	1950	28.31	18.83	10.25	11.75	10.55
61	300	1600	7.5	191.01	110.44	110.42	109.98
62	350	1450	9.19	142.44	82.24	82.26	82.22
63	400	1850	9.3	140	80.85	80.81	80.83
64	450	1700	10.91	111.06	64.1	64.15	64.12
65	500	1300	13.87	78.29	45.3	44.95	45.35
66	550	1750	13.15	84.74	48.94	48.85	48.98
67	600	1950	13.59	80.79	46.66	46.65	46.62
68	650	1800	15.32	68.04	39.2	39.25	39.4
69	700	1200	20.21	45.44	26.24	26.15	26.32
70	750	1150	22.12	39.85	23.02	22.95	23.05
71	800	1650	19.69	47.11	27.24	27.15	27.2
72	850	1050	26.23	30.65	17.98	17.85	17.25
73	900	1850	20.92	42.93	24.95	24.55	24.85
74	950	1300	26.35	28.87	17.86	17.65	17.95
75	1000	1950	22.65	38.37	22.25	22.05	22.15
76	1050	1100	31.66	23.55	13.69	13.45	13.65
77	1100	1250	31.11	24.15	14.03	13.85	13.95
78	1150	1350	31.3	23.8	13.91	13.45	13.85
79	1200	1500	30.98	24.29	14.12	13.9	14.05
80	1250	1750	29.88	25.74	14.88	14.8	14.9
81	300	1500	7.75	182.33	105.61	104.95	105.24
82	350	1950	7.93	175.74	101.52	101.32	101.55
83	400	1850	9.3	129.45	77.11	77	69.88
84	450	1100	13.57	69.715	40.27	40.15	40.33
85	500	1050	15.43	55.67	32.28	31.98	32.17
86	550	1750	13.15	73.31	42.51	42.02	42.45
87	600	1200	17.32	45.77	26.46	26.39	26.42
88	650	1400	17.37	45.6	26.33	26.3	26.35
89	700	1700	16.98	47.42	27.39	27.32	27.43
90	750	1350	20.41	34.38	19.95	19.75	19.84
91	800	1800	18.86	39.54	22.86	22.84	22.79
92	850	1300	23.57	26.87	15.57	15.45	15.52
93	900	1550	22.86	28.39	16.42	16.35	16.4
94	950	1200	27.42	20.83	12	12.05	12.02
95	1000	1950	22.65	28.85	16.69	16.66	16.62
96	1050	1900	24.09	26.02	15	15.05	15.02
97	1100	1100	33.17	13.94	8.66	8.59	8.62
98	1150	1400	30.74	15.36	8.87	8.89	8.84
99	1200	1550	30.48	17.4	10.01	10.05	10.08
100	1250	1650	30.77	15.01	9.85	9.79	9.81
101	300	1400	8.02	198.71	114.7	114.75	114.72
102	350	1250	9.9	146.44	84.85	84.82	83.97
103	400	1600	10	144.37	83.63	82.98	83.45
104	450	1150	13.27	96.67	55.81	55.78	55.84
105	500	1000	15.81	75.27	43.44	43.41	43.52
106	550	2050	12.15	109.62	63.32	63.25	63.3
107	600	1350	16.33	71.75	41.48	41.35	41.44
108	650	1250	18.38	60.52	35.01	34.85	34.96
109	700	1650	17.23	64.28	38.4	38.38	34.42
110	750	1250	21.21	49.38	28.53	28.49	28.51

Continued

Data monitoring points	Distance (m)	Charge per delay (kg)	Scaled distance (m/kg½)	PPV (mm/s)	Peak particle velocity (mm/s)		
					Vertical PPV (mm/s)	Longitudinal PPV (mm/s)	Transvers PPV (mm/s)
111	800	1900	18.35	60.73	35.1	35.03	35.06
112	850	1350	23.13	43.65	25.21	25.14	25.26
113	900	1300	24.96	39.16	22.61	22.63	22.58
114	950	1700	23.04	43.85	25.35	25.29	25.31
115	1000	1550	25.4	38.26	22.05	22.12	22.09
116	1050	1650	25.85	37.24	21.51	21.46	21.54
117	1100	1500	28.4	32.49	18.8	18.75	18.72
118	1150	1250	32.53	26.73	15.48	15.39	15.43
119	1200	1450	31.51	27.95	16.2	16.08	16.13
120	1250	1750	29.88	30.26	17.48	17.42	17.51
121	300	1050	9.26	247.53	142.91	142.94	142.89
122	350	1150	10.32	217.742	125.71	125.69	125.74
123	400	1250	11.31	195.31	112.8	112.72	112.77
124	450	1400	12.03	181.15	104.95	104.91	103.89
125	500	1450	13.13	163.81	94.62	94.58	94.53
126	550	1300	15.25	137.41	79.28	79.34	79.38
127	600	1450	15.76	131.94	76.31	75.95	76.26
128	650	1350	17.69	115.29	66.56	66.51	66.62
129	700	1650	17.23	118.47	68.65	67.93	68.62
130	750	1500	19.36	103.57	59.83	59.87	59.68
131	800	1100	24.12	79.86	46.17	46.1	46.05
132	850	1000	26.88	70.28	40.63	40.57	40.53
133	900	1300	24.96	76.87	44.34	44.39	44.42
134	950	1200	27.42	68.66	39.68	39.6	39.65
135	1000	1700	24.25	79.37	45.87	45.83	45.78
136	1050	1600	26.25	72.26	41.78	41.66	41.72
137	1100	1100	33.17	54.88	31.71	31.7	31.64
138	1150	1050	35.49	50.59	29.27	29.15	29.21
139	1200	1350	32.66	55.9	32.29	32.35	32.19
140	1250	1250	35.36	50.84	29.4	29.34	29.31
141	300	1550	7.62	138.28	79.83	79.8	79.88
142	350	1600	8.75	105.96	61.13	61.22	61.18
143	400	1650	9.85	84.19	48.67	48.53	48.62
144	450	1450	11.82	59.22	34.23	34.15	34.2
145	500	1950	11.32	64.51	37.17	37.32	37.24
146	550	1750	13.15	48.27	27.86	27.91	27.83
147	600	1550	15.24	36.21	20.95	20.87	20.9
148	650	1250	18.38	25.24	14.59	14.5	14.63
149	700	1350	19.05	23.5	13.62	13.57	13.51
150	750	1450	19.7	22.11	12.77	12.7	12.82
151	800	1450	21.01	19.45	11.27	11.22	11.19
152	850	1500	21.95	18	10.36	10.42	10.39
153	900	1600	22.5	17	9.88	9.75	9.82
154	950	1350	25.86	13.07	7.55	7.48	7.61
155	1000	1250	28.28	10.98	6.35	6.27	6.4
156	1050	1050	32.4	8.35	4.89	4.81	4.76
157	1100	1100	33.17	8	4.67	4.55	4.63
158	1150	1250	32.53	8.33	4.85	4.8	4.78
159	1200	1600	30	9.75	5.67	5.59	5.62
160	1250	1750	29.88	9.98	5.71	5.76	5.82
161	300	1200	8.66	183.69	106	106.12	106.04
162	350	1150	10.32	144.06	83.21	83.12	83.19
163	400	1800	9.43	163.19	94.28	94.15	94.22
164	450	1850	10.46	141.31	81.66	81.58	81.52
165	500	1950	11.32	126.9	73.22	73.27	73.31

Continued

Data monitoring points	Distance (m)	Charge per delay (kg)	Scaled distance (m/kg½)	PPV (mm/s)	Peak particle velocity (mm/s)		
					Vertical PPV (mm/s)	Longitudinal PPV (mm/s)	Transvers PPV (mm/s)
166	550	1450	14.44	90.52	52.33	52.26	52.2
167	600	1350	16.33	76.51	44.18	44.25	44.09
168	650	1450	17.07	71.97	41.56	41.48	41.61
169	700	1500	18.07	66.52	38.4	38.35	38.46
170	750	1750	17.93	67.26	38.83	38.79	38.88
171	800	1650	19.69	59.02	34.11	33.92	34.19
172	850	1700	20.62	55.49	32.03	32.11	31.98
173	900	1750	21.51	52.42	30.2	30.32	30.27
174	950	1600	23.75	45.55	26.34	26.25	26.3
175	1000	1850	23.25	46.77	27.13	26.85	27.02
176	1050	1400	28.06	36.12	20.93	20.79	20.84
177	1100	1450	28.89	34.93	20.11	20.23	20.16
178	1150	1350	31.3	31.35	18	18.19	18.11
179	1200	1800	28.28	35.87	20.7	20.81	20.62
180	1250	1950	28.31	35.68	20.68	20.52	20.6
181	300	850	10.29	144.74	83.56	83.47	83.66
182	350	750	12.78	107.13	61.96	61.84	61.75
183	400	1300	11.09	129.91	75.32	75.4	74.28
184	450	1100	13.57	98.97	57.05	57.22	57.15
185	500	650	19.61	59.54	34.31	34.38	34.43
186	550	1500	14.2	92.78	53.57	53.48	53.65
187	600	1750	14.34	91.49	52.84	52.72	52.9
188	650	950	21.09	53.94	31.04	31.15	31.24
189	700	1000	22.14	50.24	29.03	29.12	28.86
190	750	1300	20.8	54.8	31.63	31.56	31.72
191	800	950	25.96	40.48	23.31	23.42	23.38
192	850	950	27.58	37.23	21.44	21.56	21.49
193	900	1200	25.98	40.13	23.27	23.08	23.16
194	950	1550	24.13	44.51	25.77	25.62	25.7
195	1000	850	34.3	27.47	15.86	15.92	15.8
196	1050	1400	28.06	36.11	20.93	20.85	20.77
197	1100	1400	29.4	34.17	19.63	19.75	19.81
198	1150	700	43.47	19.69	11.44	11.29	11.38
199	1200	1600	30	33.07	19.08	19.22	18.97
200	1250	1000	39.53	22.81	13.04	13.17	13.29

Table 3. Total datasets of ground vibration measurements and design parameters for blasting from the ten-quarry site in Nigeria.

outliers or trends that might impact the accuracy of the models. Histograms provide a visual representation of the distribution of data points within a variable. By examining the shape, spread, and skewness of the histogram, we can identify unusual observations that deviate significantly from the overall pattern of the data. Specifically, outliers can often be observed as isolated bars or gaps in the histogram that are distant from the main cluster of data.

Figure 5 demonstrates the relationship between variables in terms of the scatter matrix plot. It illustrates that all variables very strongly correlate with each other. It shows a strong correlation between D and SD with ($r = 0.94$).

The violin plots of the variables are depicted in Fig. 6. It is useful for visualizing the distribution of the blasting dataset of this study, especially it describes in terms of quartiles. Quartile 1 (Q1) represents the 25th percentile, and Quartile 3 (Q3) represents the 75th percentile. The box-in-a-box plot spans from Q1 to Q3. Based on this analysis the data set in the distance shows distributed equally. Hence this is due to the monitoring station distance taking place at 50-m intervals starting from the first point up to the last 20 monitoring points with 1250 m. For SD it shows the data points are highly scattered in Q_1 and Q_3, at a range of 7 m/kg$^{1/2}$–35 m/kg$^{1/2}$. Similarly, the CPD data set is highly distributed in a range of 750–2250 kg.

Pearson and Spearman correlation coefficients are the most popular correlation coefficients in statistics, both ranging from − 1 to 1, and are frequently used to evaluate the relationship between two variables A correlation coefficient of 0 indicates no connection between variables. A positive correlation coefficient suggests a positive relationship, while a negative coefficient implies a negative relationship. The strength of the correlation is gauged by the absolute value of the coefficient; a higher absolute number indicates a stronger correlation.

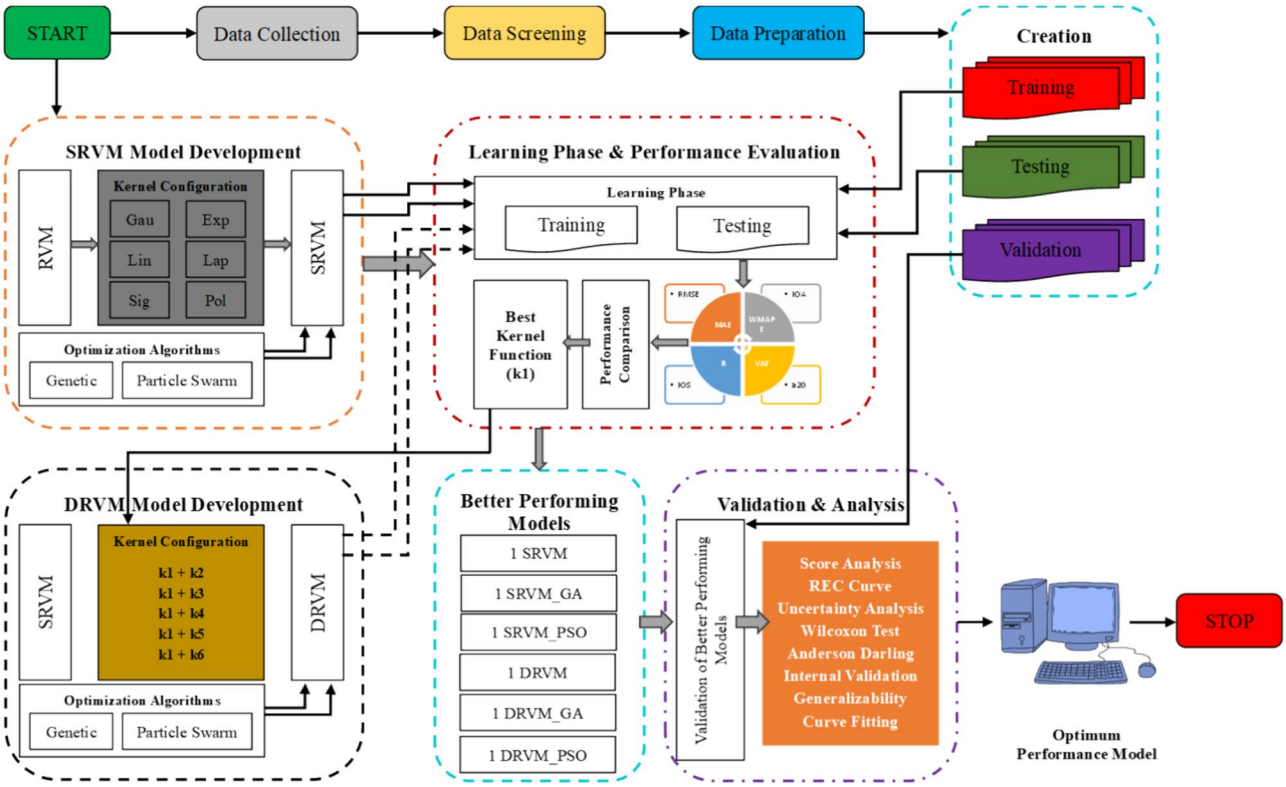

Fig. 3. Illustration of flow chart of the main research methodology.

Descriptive statistics	Distance (m)	CPD (kg)	SD (m/kg½)	PPV (mm/s)
Mean	775	1517.637	20.230	64.173
SE	20.438	25.024	0.551	3.447
Median	775	1500	19.75	46.94
Mode	300	1250	11.32	40.48
Standard deviation	289.037	353.894	7.795	48.750
Kurtosis	− 1.206	1.514	− 0.756	1.300
Skewness	0	0.551	0.194	1.355
Range	950	2300	36.5	239.53
Minimum	300	650	6.97	8
Maximum	1250	2950	43.47	247.53
Sum	155,000	303,527.5	4046.05	12,834.717
Count	200	200	200	200

Table 4. Overview of the statistical features associated with the database.

In this current study, we introduce Spearman correlation technique (Fig. 7) to capture both linear and non-linear correlation relationships among the variables. Spearman quantifies how much information about one variable can be gained by observing another. Both methods handle categorical and continuous variables. Figure 7 confirms a strong positive correlation between SD and distance with a correlation value of 0.95, and a correlation value of 0.047 between CPD and PPV, and 0.065 between distance and CPD.

During the data analysis stage, researchers use the probability (PP) plot to visualize dataset dispersion. The PP plot compares real data quantiles to predictions of a theoretical distribution, revealing the data's distribution. This graph helps determine whether data follows a probability distribution like the normal distribution. Variations from a linear trajectory in the PP plot may indicate variations from the anticipated distribution, highlighting dataset issues. For this current study, the PP plot investigates each variable (Fig. 8)**.** Based on the PP plot result variables such as CPD**,** and SD show almost good distribution in terms of the normal pattern of the data, however, the PP plot for PPV and distance shows there is no fully perfect normal distribution among the data points, some of the data points are distributed outside of the normal line. Specifically, the normal probability plot for the target variable of this study PPV indicates a mean (μ) of 64.17 and a standard deviation (σ) of 48.75 it suggests that the data is being compared or assessed in the context of a normal distribution with these specified

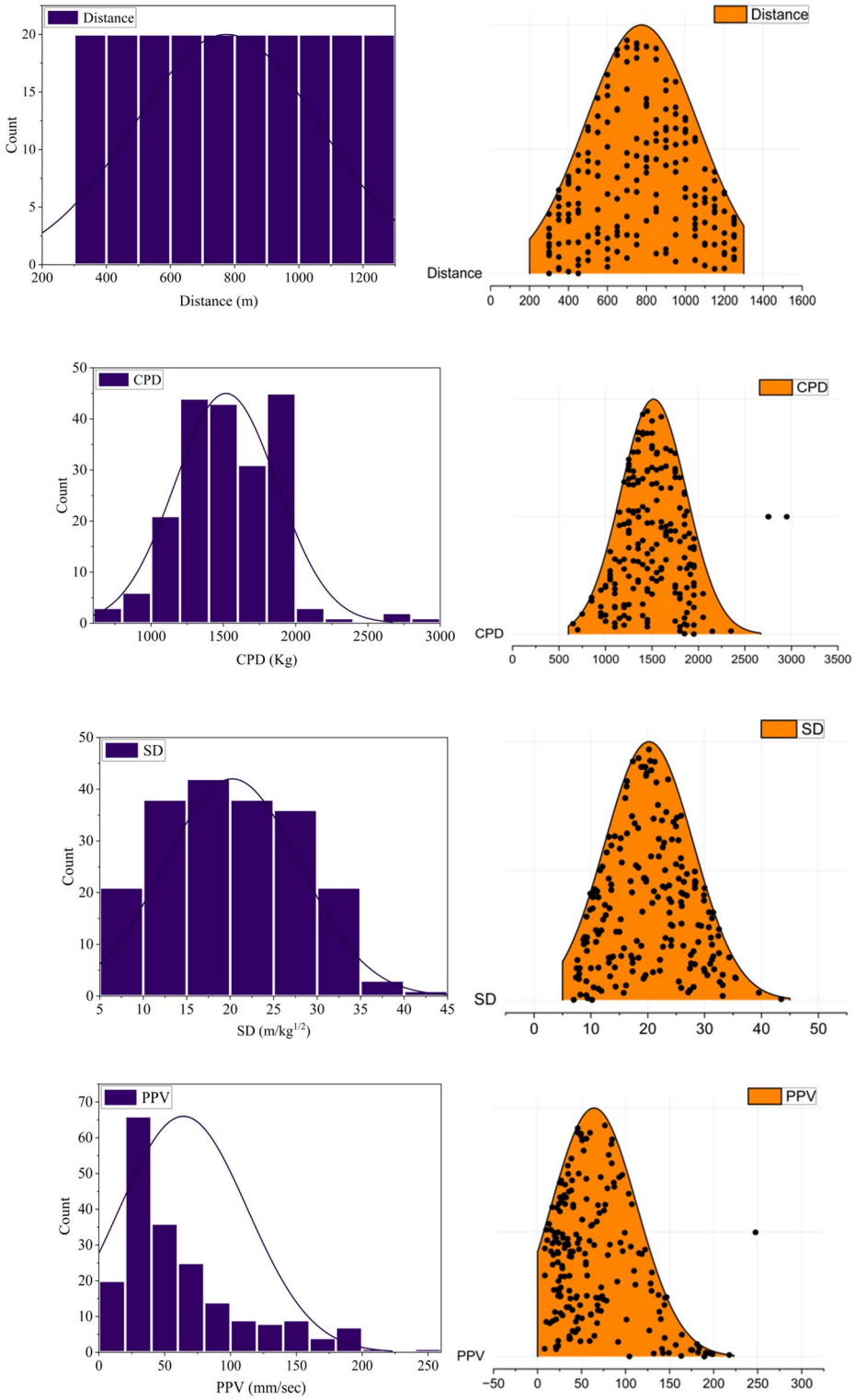

Fig. 4. Graphic representation depicting the distribution of variables based on frequency histogram plot in blue navy colour (left) and ridgeline plots in orange colour (right).

parameters. Essentially, the specified μ and σ in the normal probability plot provide a reference for assessing the normality of the dataset under consideration.

In addition to the above-advanced data analysis techniques, this study also integrates a 2D mean line graph to assess the visual depiction of data points on a coordinate system. Every point on the plot corresponds to a set of values for two variables in the blasting dataset. Examining a two-dimensional scatter plot may provide several significant observations, including the identification of patterns, detection of anomalies, and assessment

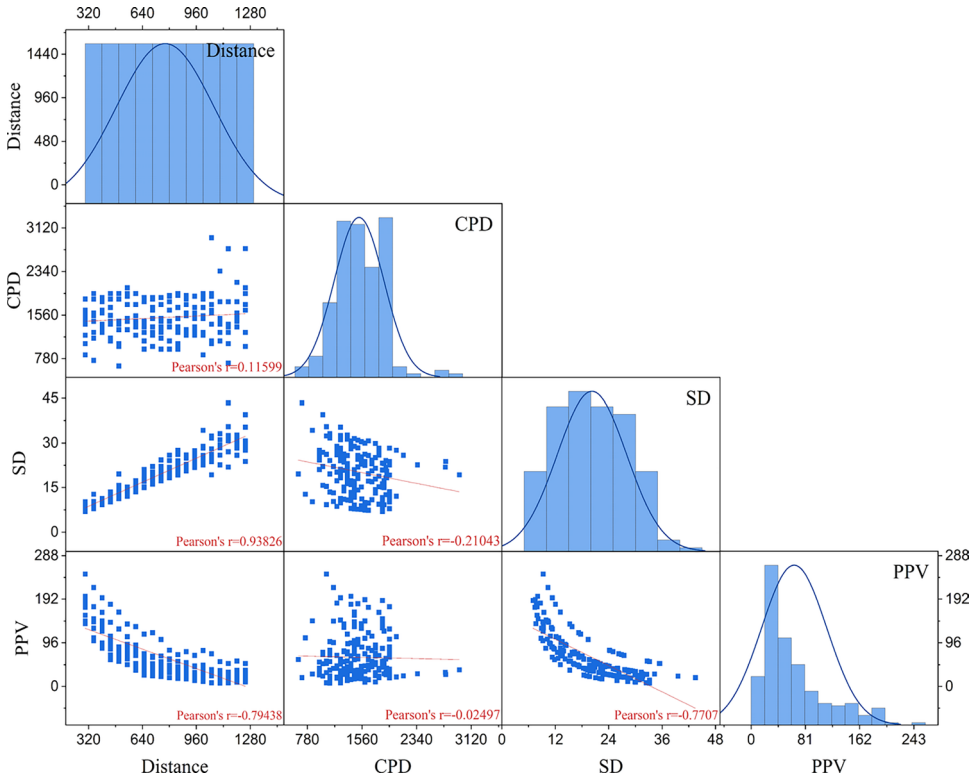

Fig. 5. Graphic representation of scatter matrix plot of all the variables to elaborate the relationship between the variables.

of data distribution**.** Based on the 2D mean line graph in Fig. 9, shows that there is almost similar data distribution among CPD and PPV. However, there is no harmonize data distribution between PPV, SD, and distance.

Soft computing approaches

This current study introduces 33 RVM models. The conventional single kernel based SRVM models were developed using polynomial, linear, sigmoid, Gaussian, exponential, and Laplacian kernel functions. Therefore, these SRVM models were optimized by each GA and PSO algorithms. Conversely, the performance of conventional SRVM models was compared to find the kernel 1 (k1). After finding k1, the different combinations of kernels were prepared. In this research, the Gaussian kernel based conventional SRVM model achieved higher performance. Hence, the following combinations were prepared to develop the dual kernel based DRVM model: (1) Gaussian + exponential, (2) Gaussian + linear, (3) Gaussian + Laplacian, (4) Gaussian + sigmoid, and (5) Gaussian + polynomial. Thus, five conventional DRVM models were developed. These five DRVM models were optimized by each PSO and GA algorithm.

Relevance vector machine (RVM)

RVM belongs to the category of kernel methods in machine learning, tailored for both regression and classification tasks. Kernel SVM, a variation of Support Vector Machine (SVM), was introduced to handle uncertainties in training data by integrating a probabilistic approach. RVM aims to address certain drawbacks present in traditional SVMs, such as difficulties in handling vast datasets and the necessity of selecting appropriate kernel functions and regularization parameters[42].

Khatti et al.[43], in their research, describe the key features of RVM, based on their analysis the main features are probabilistic framework, sparsity, kernel trick, sparse Bayesian learning, and model training. It means it is very similar to a Gaussian model with kernel (Eq. 1)

$$k(j, j\prime) = \sum_{m=1}^{n} \frac{1}{\propto m} \varphi(j, j_m)\varphi(j\prime, j_m) \tag{1}$$

where φ is the Gaussian kernel, $\propto_m$ are the variances of the prior on the weight vector ω N $(0, \alpha^{-1}I)$, and j_1,… j_N are the input variables of the training datasets[43,44]. The Gaussian

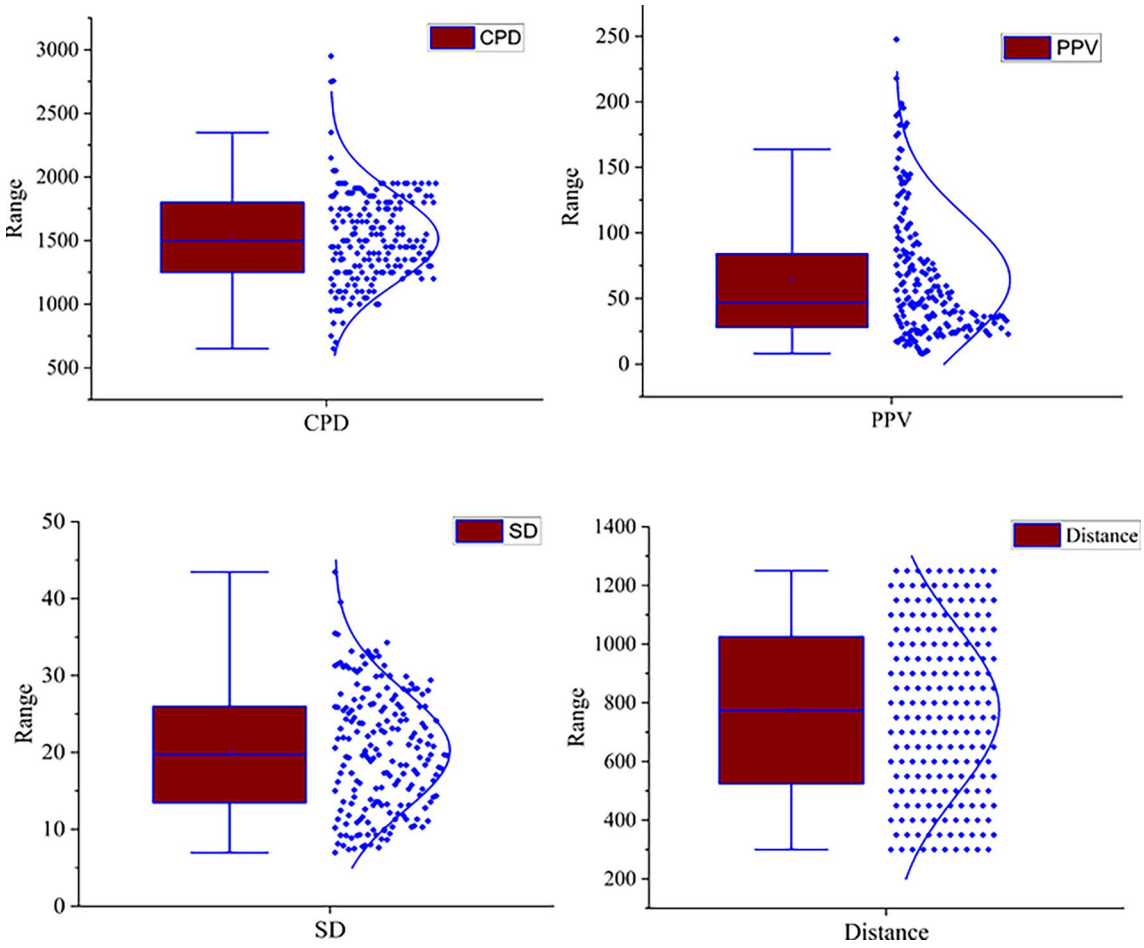

Fig. 6. Depiction of violin plots of all variables.

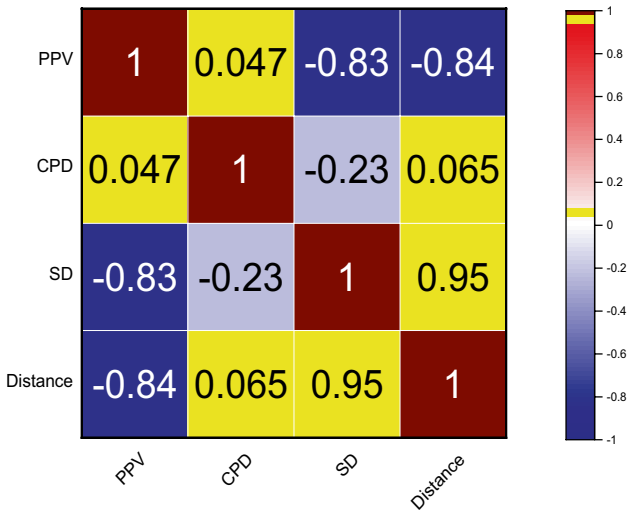

Fig. 7. Illustration of spearman correlation plot.

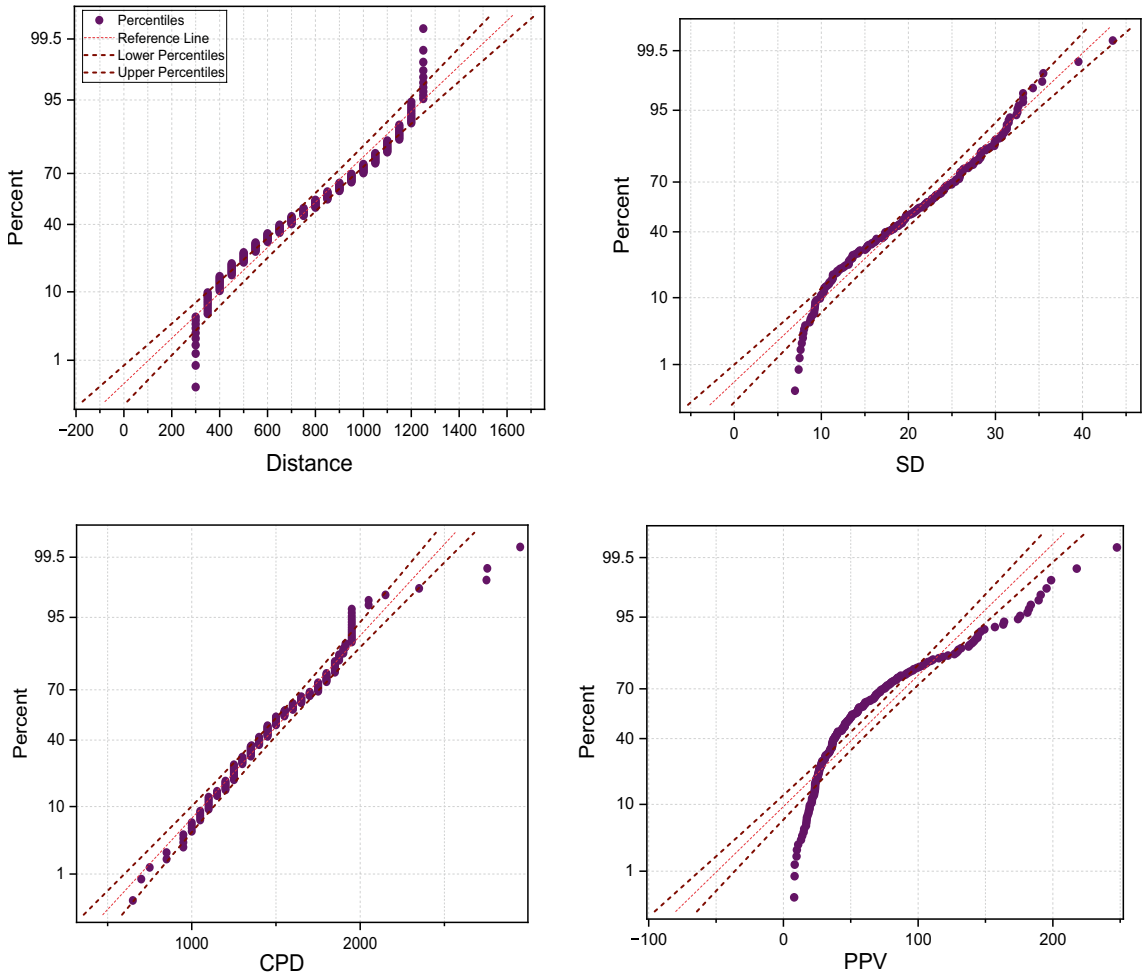

Fig. 8. Illustration of normal probability (PP) plot of all variables.

$$\left[K(x_i,x_j)=exp\left(-\frac{\|x_i-x_j\|^2}{2\sigma^2}\right),\textbf{\textit{Linear}}\left[k(x_i,x_j)=m(x_i,x_j)+c\right]\right],$$
$$\textbf{\textit{Laplacian}}\left[K(x_i,x_j)=\exp\left(-\frac{\|x_i-x_j\|}{\sigma}\right)\right], \quad (2)$$
$$\textbf{\textit{Polynomial}}\left[k(x_i,x_j)=(x_i\cdot x_j+1)^d\right],\textit{and}\ \textbf{\textit{Exponential}}\left[k(x_i,x_j)=D^2exp\left(-\frac{\|x_i-x_j\|}{l}\right)\right]$$

kernels have developed the RVM models in the present study (Eq. 2). The x_i, x_j are the basic input and out variables, c is constant, m is the gradient/slope of a line, d is the degree, D is the scale factor, 1 is the length scale hyper-parameter, and σ is the standard deviation.

Therefore, for the first time this study introduced RVM models for predicting the ground vibration (PPV), a total of six RVM models were implemented for predicting the PPV. These are 6 single kernel-based RVM conventional models (SRVM), 5 dual kernel-based RVM conventional models (DRVM), 6 GA-optimized single kernel-based RVM models (GA_SRVM), 6 PSO-optimized single kernel-based RVM models (PSO_SRVM), 5 GA-optimized Dual kernel-based RVM models (GA_DRVM), and 5 PSO-optimized Dual kernel-based RVM models (PSO_DRVM).

Two types of kernel function based RVM models have been developed for PPV prediction: single (SRVM) and dual (DRVM) models. Table 5 presents the RVM model configurations that were developed. This research has created 33 RVM models by using the hyperparameters specified in Table 5.

Sensitivity analysis (SA)

The study employs sensitivity analysis (SA) to pinpoint the most influential independent variables in regression or numerical prediction models. Eliminating insignificant input parameters is crucial for improving model performance. In this research, the cosine amplitude technique (CAM) is utilized for SA. Figure 10 shows that charge per delay has the highest influence score of 0.772, followed by distance at 0.579 and scaled distance at 0.577. In Eq. 3, the vector x (of length m) represents the predictors x_i in the data array is specified as follows.

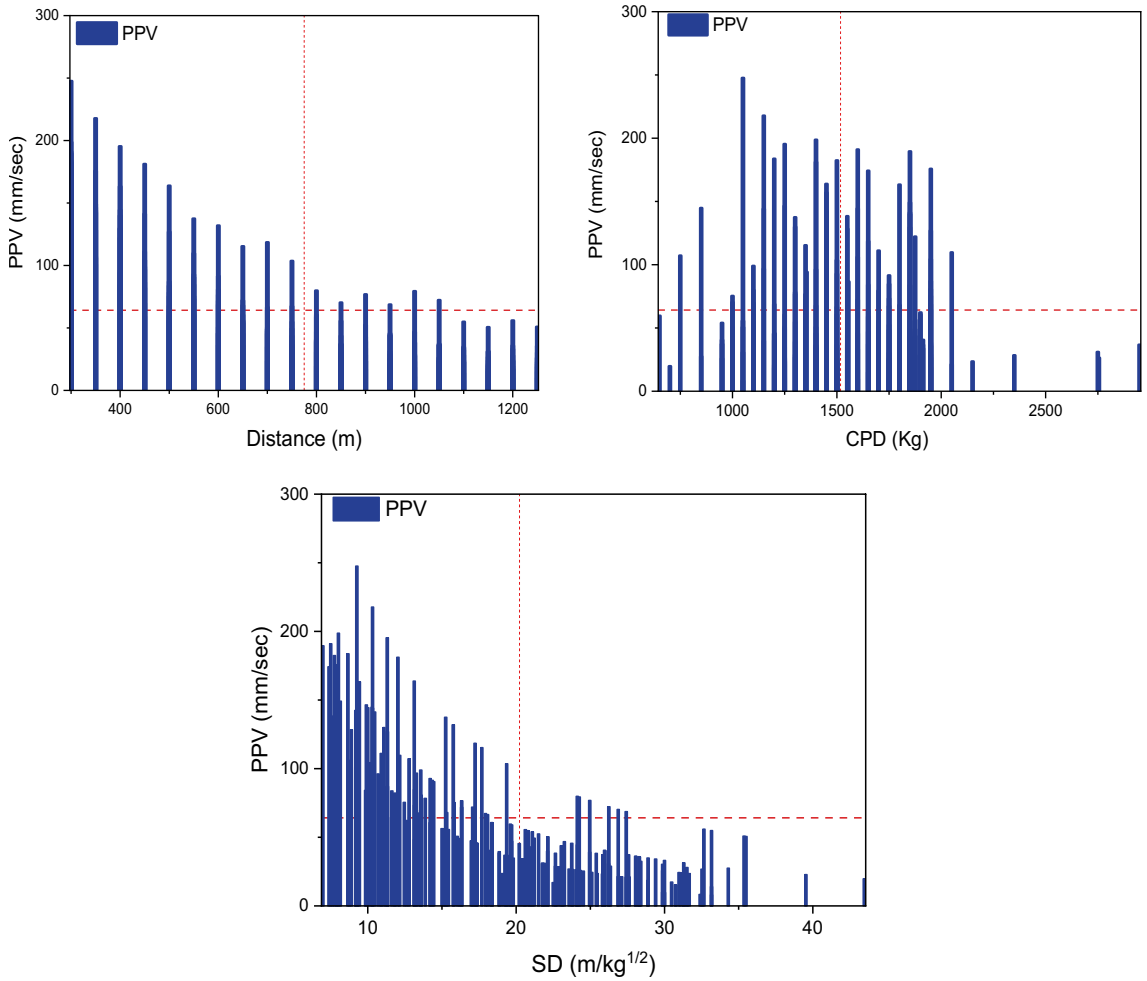

Fig. 9. Depiction of 2D mean line graph plot of each input variable (y-axis) with the target variable (x-axis) to illustrate the interaction between each variable.

Hyperparameters	SRVM model	DRVM model
Parameter settings		
Kernel functions	Linear, Polynomial, Gaussian	and Laplacian
Maximum iterations	1000	1000
Number of kernels	Single	Two
Free basis	Enable	Enable
Optimizer settings		
Methods	GA and PSO	GA and PSO
Target	Single kernel	Dual kernel
Lb	2–6	$2^{-5}, 10^{-2}, 10^{-3}, 10^{-3}$
uB	2–6	$2^{-5}, 10^{0}, 10^{3}, 10^{3}$
Num. variable	1	4
Maximum iterations	100	100
k-folds	5	5

Table 5. Basic RVM model hyperparameters configured with a k-fold value of 5.

$$X = \{x_{i1}, x_{i2}, x_{i3}, \ldots x_{in}\} \tag{3}$$

In Eq. (4), the significance between predictors (x_i) and targets (x_j) is estimated[45].

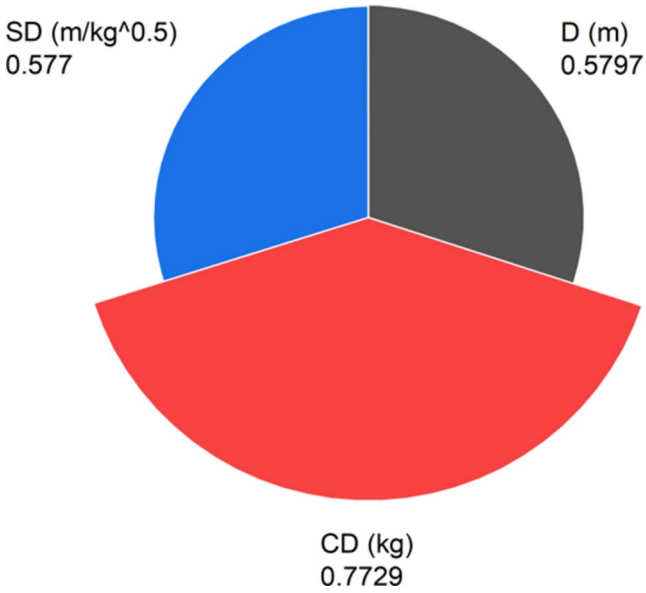

Fig. 10. Depiction of cosine amplitude sensitivity analysis (SA) for input variables.

$$\mathrm{CASA} = \frac{\sum_{k=1}^{m} x_{ik} x_{jk}}{\sqrt{\sum_{k=1}^{m} x_{ik}^2 \sum_{k=1}^{m} x_{jk}^2}} \tag{4}$$

In this study correlation plots and sensitivity analysis serve different purposes. Correlation plots visualize the relationship between variables, showing the strength and direction of linear or non-linear relationships through correlation coefficients. They are useful for identifying patterns within a dataset. For this target this study introduces different correlation plots such as Pearson and spearman correlation plots (see Figs. 5 and 7). Sensitivity analysis, on the other hand, assesses how variations in input variables affect the output of a model. It quantifies the impact of each variable, aiding in model validation and decision-making by identifying critical variables. In our current study we introduced cosine amplitude sensitivity analysis based on this CPD shows higher influence on the output with 0.77.

Performance evaluation

The current study has used the following eleven basic metrics to assess the performance of models: (1) Root means square error (*RMSE*), (2) Mean absolute percentage error (*MAPE*), (3) Mean absolute error (*MAE*), (4) Weighted Mean Absolute Percentage Error (*WMAPE*), (5) Correlation coefficient (*R*), (6) Variance account for (*VAF*), (7) Nash–Sutcliffe Efficiency (NS), (8) Ratio of Standard Deviation (RSR), and (9) the Bias factor (BF), (10) Performance index (PI), (11) Index of scatter (IOS), (12) Index of agreement (IOA), (13) Normalized mean bias error (NMBE), (14) Legate and McCabe's index (LMI), (15) a20-index (a20), and (16) Mean bias error (NMBE)[42]. All the performance evaluation equations are included starting from Eqs. (5) to (20).

$$\mathrm{RMSE} = \sqrt{\frac{1}{\mathrm{n}} \sum_{\mathrm{i}=1}^{\mathrm{n}} (\alpha - \beta)^2} \tag{5}$$

$$\mathrm{MAE} = \frac{1}{\mathrm{n}} \sum_{\mathrm{i}=1}^{\mathrm{n}} (|\omega - \alpha|) \tag{6}$$

$$\mathrm{WMAPE} = \frac{\sum_{\mathrm{i}=1}^{\mathrm{n}} \left| \frac{\alpha - \omega}{\alpha} \right| * \alpha}{\sum_{\mathrm{i}=1}^{\mathrm{n}} \alpha} \tag{7}$$

$$\mathrm{MAPE} = \frac{1}{\mathrm{n}} \sum_{\mathrm{i}=1}^{\mathrm{n}} \left| \frac{\alpha - \omega}{\alpha} \right| * 100 \tag{8}$$

$$\mathrm{IOA} = 1 - \frac{\sum_{\mathrm{i}=1}^{\mathrm{n}} (\omega - \alpha)}{2 \sum_{\mathrm{i}=1}^{\mathrm{n}} (\omega - \beta)} \tag{9}$$

$$\mathrm{IOS} = \frac{\mathrm{RMSE}}{\text{Average of actual values}} \tag{10}$$

$$\mathrm{PI} = \mathrm{R}^2 + \left(\frac{\mathrm{VAF}}{100}\right) - \mathrm{RMSE} \tag{11}$$

$$\mathrm{BF} = \frac{1}{\mathrm{N}} \sum_{\mathrm{i}=1}^{\mathrm{n}} \frac{\alpha}{\omega} \tag{12}$$

$$\mathrm{LMI} = 1 - \left[\frac{\sum_{\mathrm{i}=1}^{\mathrm{n}} |\alpha - \omega|}{\sum_{\mathrm{i}=1}^{\mathrm{n}} |\alpha - \beta|}\right] \tag{13}$$

$$\mathrm{NMBE} = \frac{\frac{1}{\mathrm{N}} \sum_{\mathrm{i}=1}^{\mathrm{n}} (\omega - \alpha)^2}{\frac{1}{\mathrm{N}} \sum_{\mathrm{i}=1}^{\mathrm{n}} \alpha} \tag{14}$$

$$\text{a20 index} = \frac{\mathrm{m20}}{\mathrm{H}} \tag{15}$$

$$\mathrm{NS} = 1 - \frac{\sum_{\mathrm{i}=1}^{\mathrm{n}} (\alpha - \omega)^2}{\sum_{\mathrm{i}=1}^{\mathrm{n}} (\alpha - \beta)^2} \tag{16}$$

$$\mathrm{RSR} = \frac{\mathrm{RMSE}}{\sqrt{\frac{1}{\mathrm{N}} \sum_{\mathrm{i}=1}^{\mathrm{N}} (\alpha - \beta)^2}} \tag{17}$$

$$\mathrm{VAF} = \left(1 - \frac{\mathrm{var}(\alpha - \omega)}{\mathrm{var}(\alpha)}\right) * 100 \tag{18}$$

$$\mathrm{R} = \frac{\sum \left(\alpha - \overline{\beta}\right)(\omega_{\mathrm{i}} - \overline{\omega})}{\sqrt{\sum \left(\alpha_{\mathrm{i}} - \overline{\beta}\right)^2 \sum (\omega_{\mathrm{i}} - \overline{\omega})^2}} \tag{19}$$

$$\mathrm{MBE} = \frac{1}{\mathrm{N}} \sum_{\mathrm{i}=1}^{\mathrm{n}} (\omega - \alpha) \tag{20}$$

The variables **α** and **ω** represent the actual and predicted **i**-th values respectively. The variable n represents the total number of data points. **β** represents the mean of the actual values, while $\overline{\boldsymbol{\omega}}$ represents the mean of the predicted values. The variable k represents the number of independent variables. The variable m20 represents the ratio of experimental to predicted values, which can vary between 0.8 and 1.2. H represents the total number of data samples.

The main benefit of the a20-index is its ability to predict the values within a deviation range of ± 20% in comparison to the actual measured values. Conversely, the index of agreement is limited to a range of – 1.0 to 1.0n[46]. A perfect predictive model always has performance indicators value equal to the ideal value, as given in Table 6.

Metrics	Value	Metrics	Value
R^2	1	RMSE	0
R	1	MAE	0
MAPE	0–100	WMAPE	0
VAF	100	PI	2
NMBE	0	NS	1
LMI	0	RSR	0
a20-index	100	IOA	0
BF	0	IOS	0

Table 6. Main values of the different evaluation metrics in machine learning.

Model	Phase	RMSE	MAE	R	MAPE	VAF	WMAPE	NS	PI	BF	NMBE	WI	MBE	LMI	RSR	a20	IOA	IOS
MD1	Train	21.9662	15.8079	0.8948	0.3445	80.06	0.2530	0.8006	1.51	1.1668	7.7234	0.9974	0.0341	0.4212	0.4466	56.25	0.7894	0.3516
	Test	25.2820	17.7599	0.8854	0.2388	78.35	0.2119	0.7693	1.46	0.9772	7.6248	0.9965	-6.2726	0.3855	0.4803	55.00	0.8072	0.3016
	Valid	22.5340	16.9839	0.7770	0.3467	54.28	0.2922	0.5265	1.05	1.1605	8.7375	0.9929	4.1799	0.6113	0.6881	30.00	0.6943	0.3877
MD10	Train	21.9575	15.7224	0.8949	0.3502	80.07	0.2517	0.8007	1.51	1.1661	7.7173	0.9974	0.0341	0.4189	0.4464	45.63	0.7906	0.3515
	Test	25.6335	18.0084	0.8820	0.2407	77.70	0.2148	0.7629	1.45	0.9755	7.8383	0.9961	-6.2585	0.3909	0.4869	50.00	0.8045	0.3058
	Valid	22.5340	16.9839	0.7770	0.3467	54.28	0.2922	0.5265	1.05	1.1605	8.7375	0.9929	4.1799	0.6113	0.6881	30.00	0.6943	0.3877
MD16	Train	20.4599	14.8188	0.9094	0.3451	82.70	0.2372	0.8270	1.57	1.1673	6.7005	0.9977	0.0341	0.3948	0.4159	48.75	0.8026	0.3275
	Test	25.2460	18.6492	0.8799	0.2791	77.35	0.2225	0.7700	1.44	1.0767	7.6031	0.9959	-3.1068	0.4048	0.4796	52.00	0.7976	0.3012
	Valid	22.5340	16.9839	0.7770	0.3467	54.28	0.2922	0.5265	1.05	1.1605	8.7375	0.9929	4.1799	0.6113	0.6881	30.00	0.6943	0.3877
MD21	Train	22.6713	15.5568	0.8875	0.3473	78.76	0.2490	0.7876	1.48	1.1695	8.2272	0.9974	0.0341	0.4145	0.4609	48.13	0.7928	0.3629
	Test	25.8582	18.5053	0.8776	0.2479	76.87	0.2208	0.7587	1.43	0.9921	7.9763	0.9960	-5.2581	0.4017	0.4912	52.00	0.7991	0.3085
	Valid	21.6117	15.5094	0.7544	0.3545	56.88	0.2669	0.5645	1.05	1.1439	8.0369	0.9901	-2.1526	0.5583	0.6599	50.00	0.7209	0.3719
MD26	Train	20.4729	14.9638	0.9093	0.3435	82.68	0.2395	0.8268	1.57	1.1613	6.7091	0.9976	0.0341	0.3987	0.4162	49.38	0.8007	0.3277
	Test	24.3589	18.2533	0.8872	0.2861	78.64	0.2177	0.7859	1.47	1.1110	7.0782	0.9962	-1.1517	0.3963	0.4627	45.00	0.8019	0.2906
	Valid	22.1191	16.0132	0.7603	0.3405	54.39	0.2755	0.5438	1.03	1.1246	8.4187	0.9920	0.2884	0.5764	0.6754	55.00	0.7118	0.3806
MD29	Train	20.2579	14.6322	0.9114	0.3427	83.04	0.2342	0.8304	1.58	1.1437	6.5689	0.9977	-0.2653	0.3898	0.4118	60.00	0.8051	0.3243
	Test	21.2999	16.2272	0.9175	0.2094	83.92	0.1936	0.8363	1.59	0.9750	5.4120	0.9967	-2.8230	0.3523	0.4046	65.00	0.8239	0.2541
	Valid	18.5467	13.4658	0.8369	0.3055	67.99	0.2317	0.6793	1.30	1.1144	5.9189	0.9941	0.8088	0.4847	0.5663	60.00	0.7577	0.3191

Table 7. Results obtained from the soft computing models in the training and testing phase.

Results and discussion

In this study total six models are selected from the thirty-three total models i.e. MD1, MD10, MD16, MD21, MD26, and MD29 based on their different kernel configurations. The conventional single kernel based SRVM models were developed using linear, polynomial, Gaussian, sigmoid, exponential, and Laplacian kernel functions. Therefore, these SRVM models were optimized by each GA and PSO algorithm. Conversely, the performance of conventional SRVM models was compared to find the kernel 1 (k1). After finding k1, the different combinations of kernels were prepared. In this research, the Gaussian kernel based conventional SRVM model achieved higher performance. Hence, the following combinations were prepared to develop the dual kernel based DRVM model: (1) Gaussian + exponential, (2) Gaussian + linear, (3) Gaussian + Laplacian, (4) Gaussian + sigmoid, and (5) Gaussian + polynomial. Thus, five conventional DRVM models were developed. These five DRVM models were optimized by each GA and PSO algorithm. 6 single kernel-based RVM conventional models (SRVM), 5 dual kernel-based RVM conventional models (DRVM), 6 GA-optimized single kernel-based RVM models (GA_SRVM), 6 PSO-optimized single kernel-based RVM models (PSO_SRVM), 5 GA-optimized Dual kernel-based RVM models (GA_DRVM), and 5 PSO-optimized Dual kernel-based RVM models (PSO_DRVM) approaches have been employed, performed, and analysed. The seventeen-evaluation metrics have measured the training (TR) and testing (TS) performances of all models, as summarized in Table 7. Table 7 demonstrates that the PSO-optimized Dual kernel-based RVM models (PSO_DRVM) model MD29 has higher performance (TS = 0.9175, TR = 0.9114) than other RVM models. It has been measured that model MD29 predicts the ground vibration with RMSE = 21.299 mm/s, MAE = 16.2272 mm/s, MAPE = 0.2094 mm/s, WMAPE = 0.1936 mm/s, and NMBE = 5.4120, in the TS phase. The comparison shows that model MD29 predicts ground vibration with the least residuals in the TR and TS phases. In similar style the results obtained from the soft computing models in the training, validation and testing phase include the different models and seventeen metrics are shown in Table 8.

The overall comparison reveals that MD29 (DRVM_PSO with Gaussian + Exponential kernel) is the optimum performance model for assessing the ground vibration during blasting. A statistical relationship is drawn between actual and predicted PPV using models MD1, MD10, MD16, MD21, MD26, and MD29, as depicted in Fig. 11.

Score analysis

The evaluation of computational models' effectiveness is conducted through score analysis, employing statistical methods. Each model is assigned a score, denoted as 'n', indicating its ability to accurately determine optimal values for performance indicators. This study utilized a sample size of 6 and focused on soft computing models. The highest and lowest values of performance indicators in the score analysis represent the best and worst training and testing instances for the models. The overall model score is determined by averaging the scores of performance indicators across both training and testing phases.

The testing and training results are used to get the overall score of a model. The score analysis findings for the training and testing performances of the computational models MD1, MD10, MD16, MD21, MD26, and MD29 are summarized and shown in Fig. 12.

Model	Phase	RMSE	MAE	R	MAPE	VAF	WMAPE	NS	PI	BF	NMBE	WI	MBE	LMI	RSR	a20	IOA	IOS	Total
MD1	Train	2	1	2	4	2	1	2	2	4	2	1	4	1	2	5	1	2	38
	Test	3	5	4	5	4	5	3	4	3	3	5	6	5	3	5	5	3	71
	Valid	1	1	3	4	1	1	1	3	4	1	5	2	1	1	1	1	1	32
MD10	Train	3	2	3	1	3	2	3	3	3	3	3	2	2	3	1	2	3	42
	Test	2	4	3	4	3	4	2	3	2	2	3	5	4	2	2	4	2	51
	Valid	2	2	3	3	2	2	2	4	5	2	4	1	2	2	1	2	2	41
MD16	Train	5	5	5	3	5	5	5	5	5	5	5	3	5	5	3	5	5	79
	Test	4	1	2	2	2	1	4	2	5	4	1	3	1	4	3	1	4	44
	Valid	3	3	5	2	3	3	3	5	6	3	3	3	3	3	1	3	3	55
MD21	Train	1	3	1	2	1	3	1	1	6	1	2	1	3	1	2	3	1	33
	Test	1	2	1	3	1	2	1	1	4	1	2	4	2	1	3	2	1	32
	Valid	5	5	1	1	5	5	5	2	3	5	1	6	5	5	4	5	5	68
MD26	Train	4	4	4	5	4	4	4	4	2	4	4	5	4	4	4	4	4	68
	Test	5	3	5	1	5	3	5	5	6	5	4	1	3	5	1	3	5	65
	Valid	4	4	2	5	4	4	4	1	2	4	2	5	4	4	5	4	4	62
MD29	**Train**	**6**	**6**	**6**	**6**	**6**	**6**	**6**	**6**	**1**	**6**	**6**	**6**	**6**	**6**	**6**	**6**	**6**	**97**
	Test	**6**	**6**	**6**	**6**	**6**	**6**	**6**	**6**	**1**	**6**	**6**	**2**	**6**	**6**	**6**	**6**	**6**	**93**
	Valid	**6**	**6**	**6**	**6**	**6**	**6**	**6**	**6**	**1**	**6**	**6**	**4**	**6**	**6**	**6**	**6**	**6**	**95**

Table 8. Results obtained from the soft computing models in the training and testing phase include the different models and seventeen metrics. Bold shows values correspond to the best model having good prediction results.

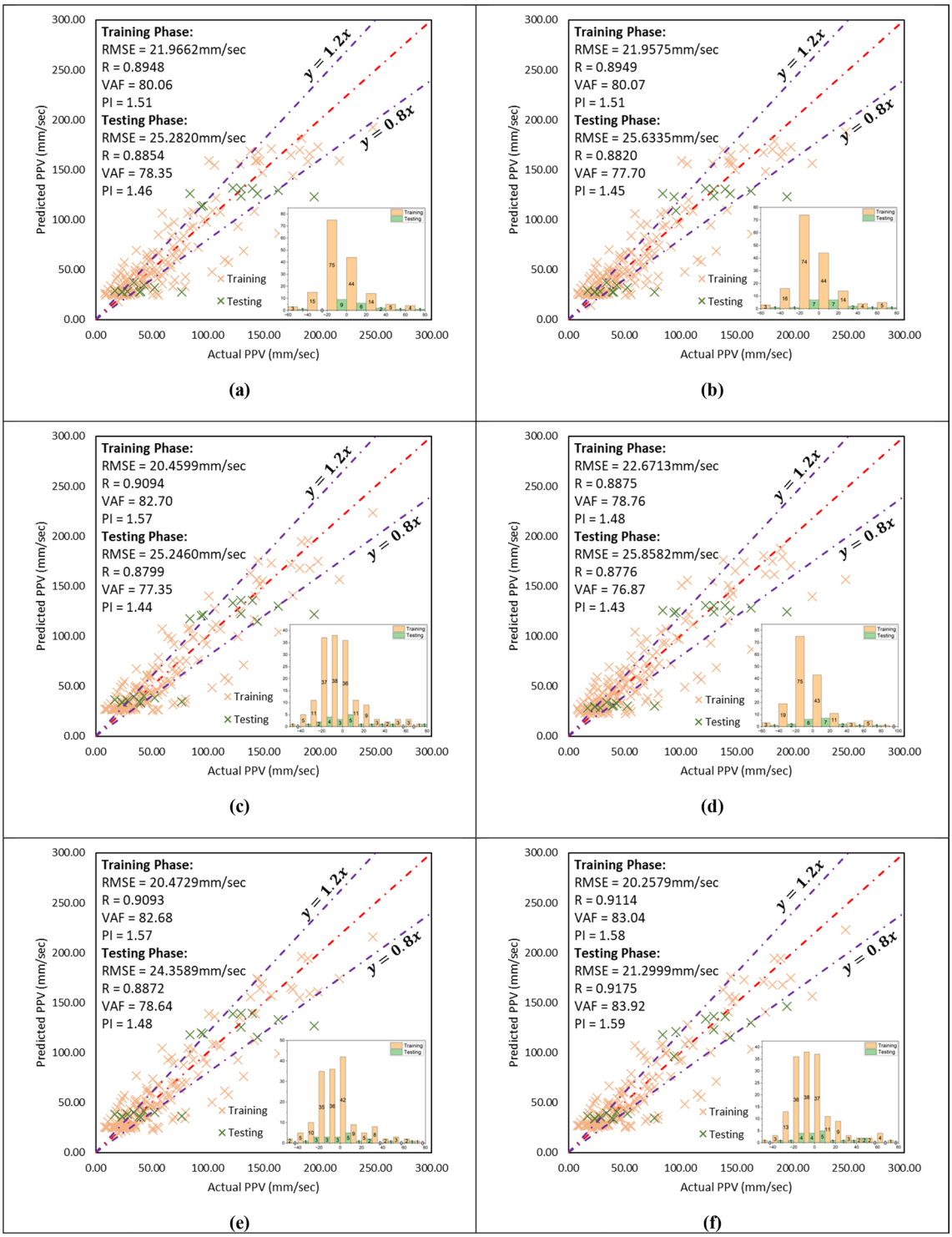

Fig. 11. Illustration of the relationship between actual and predicted PPV using RVM models (**a**) MD1, (**b**) MD10, (**c**) MD16, (**d**) MD21, (**e**) MD26, and (**f**) MD29.

Figure 12 illustrate that MD29 exhibits superior performance in both training and testing phases. Consequently, MD29 emerges as the most effective model for assessing ground vibration PPV resulting from blasting activities. In contrast, MD21 is identified as the poor performing model in this study, given its lowest score.

Regression error characteristics (REC) curve

The REC curve is a visual tool that effectively illustrates the distribution of prediction errors, offering valuable insights into the performance of regression models. The REC curve differs from conventional metrics like MSE or MAE by emphasizing the cumulative distribution function of the absolute errors. The function graphs the

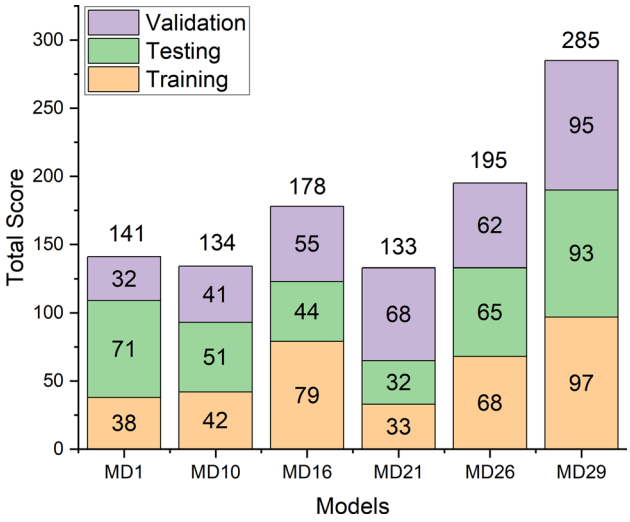

Fig. 12. Total score of better performing models.

ratio of occurrences with errors that are less or equal to a specified threshold, versus that threshold. REC curves extend the concept of ROC curves to regression problems. The y-axis of REC curves displays the proportion of projected points that are inside the specified error tolerance, while the x-axis represents the error tolerance. The resultant curve offers an approximation of the cumulative distribution function of the error. The current study included the creation of REC curves for testing, training, and validation of several RVM models.

These curves are shown in Fig. 13, along with the corresponding AOC values listed in Table 9.

Table 8 indicates that model MD29 achieved the lowest AOC values. Specifically, it obtained an AOC of 6.84E−03 during training, 6.85E−03 during testing, and 5.20E−03 during validation. These values are like the AOC of the real ground vibration. Therefore, model MD29 is a model that delivers optimal performance.

Curve fitting

In this study, six RVM models, i.e. MD1, MD10, MD16, MD21, MD26, and MD29, have been developed. MD29 is recognized as the better-performing model in predicting the PPV. Models MD1, MD10, MD16, MD21, MD26, and MD29 have been trained by 70%, 80%, 70%, 50%, 70%, 80%, 70%, 60%, 50%, and 100% training databases, respectively.

Based on Fig. 14, the overfitting comparison shows that model MD29 performs well with the lowest overfitting of 1.05 in the testing phase and 0.92 in the validation phase.

Illustrations of Taylor plots for (a) testing, (b) training, and (c) validation phase have been found in Fig. 15. Taylor plots offer invaluable advantages for predicting blasting vibration. They provide a clear visual representation of the relationship between predicted and observed values, facilitating easy interpretation and assessment of model performance. Through quantitative measures like correlation coefficient and standard deviation ratio, Taylor plots enable analysts to gauge the accuracy and precision of predictive models. Moreover, they pinpoint systematic bias and variability, aiding in model refinement and improvement. Taylor plots also allow for the comparison of multiple models on the same graph, facilitating informed decisions about model selection. Ultimately, they serve as a diagnostic tool for enhancing predictive accuracy and reliability, making them indispensable in the field of blasting vibration prediction.

Anderson–Darling (AD) test

The Anderson–Darling (AD) test is a statistical tool used to assess whether a given dataset conforms to a particular probability distribution, particularly focusing on extreme values. It is commonly employed to evaluate normality, comparing the observed data to a theoretical distribution, often the normal (Gaussian) distribution. The research hypothesis (HR) suggests that the data deviate from the specified distribution, while the null hypothesis (H0) contends that the data are drawn from that distribution. A lower AD test statistic indicates a stronger alignment with the specified distribution. In our study, we applied the AD test to evaluate the fit of actual data and predictions from several models (MD1, MD10, MD16, MD21, MD26, and MD29), as depicted in Fig. 16. Notably, model MD29 exhibited an AD value of 11.607 for predicting the ground vibration PPV closely matching the actual PPV dataset. The AD test results support the hypothesis of a normal distribution and suggest that MD29 performs best among the models examined.

Wilcoxon test

The Wilcoxon test includes two variations: the rank sum test and the signed-rank test. These tests are used to assess and compare two groups that have been effectively matched. The Wilcoxon test is used to evaluate the presence of a statistically significant difference between two or more sets of paired data. The Wilcoxon test was used on the RVM models to predict the PPV of the blasting in both the testing, and training phases. Table 10

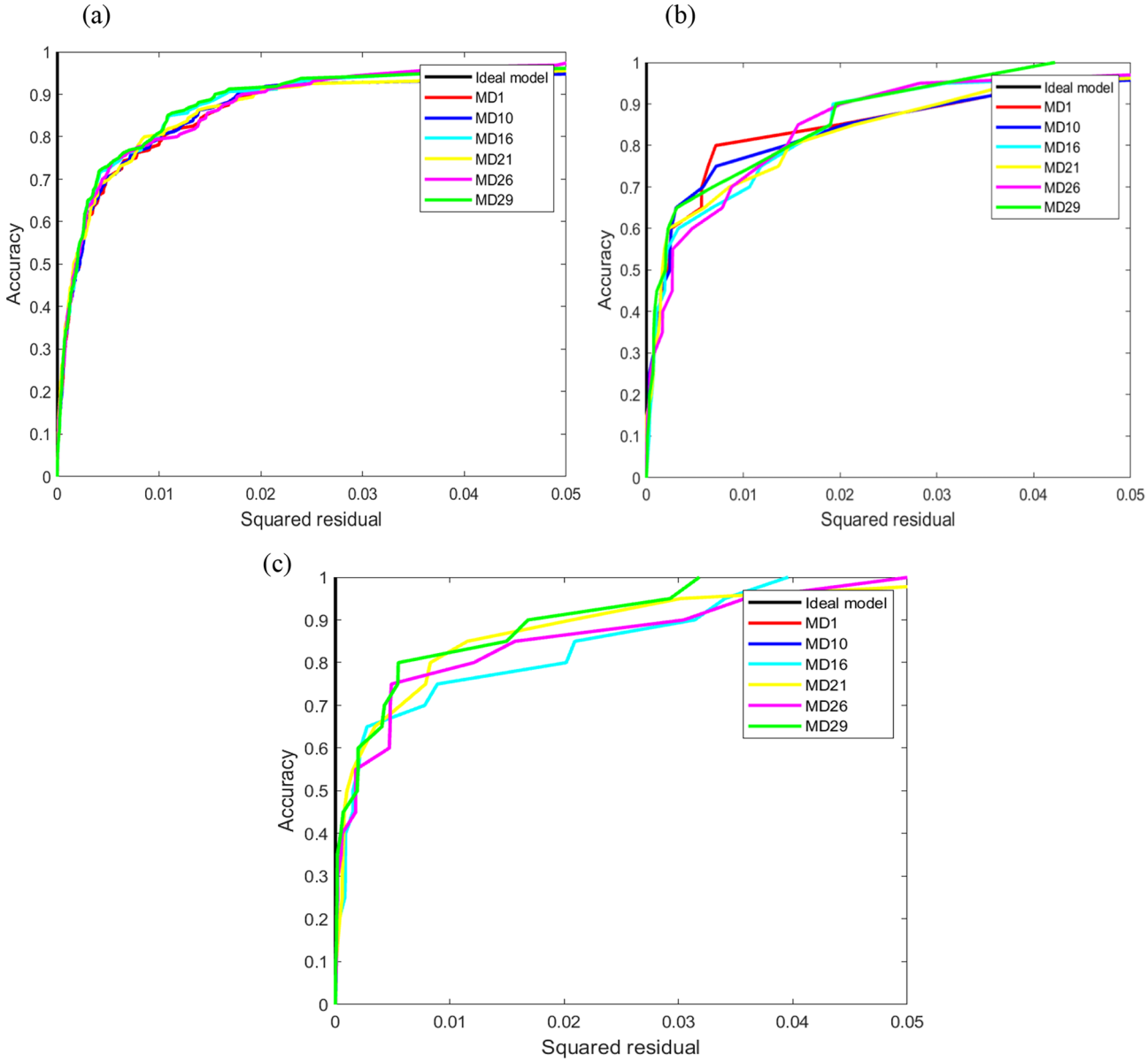

Fig. 13. Depiction of AOC results for (**a**) training and (**b**) testing, (**c**) validation phase.

	Actual	MD1	MD10	MD16	MD21	MD26	MD29
Train	0.00E + 00	8.08E − 03	8.07E − 03	6.98E − 03	8.51E − 03	6.98E − 03	**6.84E − 03**
Test	0.00E + 00	8.85E − 03	9.16E − 03	8.75E − 03	9.44E − 03	8.28E − 03	**6.85E − 03**
Valid	0.00E + 00	7.86E − 03	7.86E − 03	7.86E − 03	6.49E − 03	7.27E − 03	**5.20E − 03**

Table 9. AOC values for soft computing models for training, testing, and validation. Bold blue values present the optimum performance model.

presents the results of the Wilcoxon test. The table indicates that throughout the training phase, model MD29 made accurate predictions of the PPV, with a different confidence interval (CI). This confidence range is comparable to the confidence interval of the true PPV of the blasting in the testing database. In the training phase, model MD29 assessed the PPV with a confidence interval of 0.2240 (upper bound) and 0.1596 (lower bound). The confidence interval (CI) of the actual test database is quite like this CI, with an upper level of 0.4140 and a lower level of 0.1333. The findings indicate that model MD29 has superior performance compared to the MD1, MD10, MD16, MD21, and MD26.

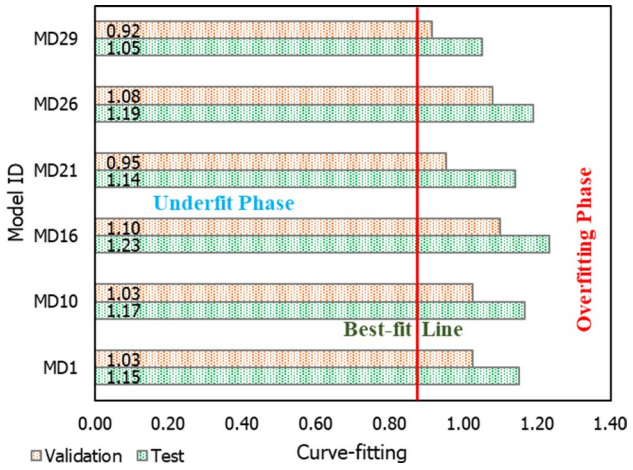

Fig. 14. Illustration of curve fitting of the six RVM models, MD1, MD10, MD16, MD21, MD26, and MD29.

Uncertainty analysis (UA)

Assessing the reliability of soft computing models is crucial for accurately predicting results, particularly in scenarios like projecting the PPV resulting from quarry blasting. This study employs UA to gauge the prediction error of the utilized models across both training and testing phases. A comparison between predicted outputs and actual data points is imperative to evaluate model reliability, for which UA proves highly suitable. This analysis involves computing various statistical measures such as absolute error, margin of error (MOE), standard deviation (StDev), standard error (SE), margin of error at a 95% confidence level (ME), white blood cell count (WBC), upper bound (UB), and lower bound (LB). The findings are subsequently documented in Table 11. A successful model regularly demonstrates a reduced WCB value[47].

Table 11 indicates that models MD1, MD10, MD16, MD21, MD26, and MD29 both for training, testing, and validation in the uncertainty analysis, with MD29 getting the highest position. The width of the confidence bound (WCB) of various models has been examined to establish the most accurate architectural model for predicting the positive predictive value PPV of blasting.

In comparing the computational costs of different algorithms for predicting PPV resulting from blasting vibrations. While simpler algorithms like linear regression offer relatively fast computation times, they often struggle to capture the intricacies of the geological and blasting parameters that influence PPV accurately. Conversely, more sophisticated methods such as RVM or ensemble techniques like random forests may demand higher computational resources due to their complexity, especially during model training and optimization. Moreover, employing advanced techniques like convolutional neural networks (CNNs) for predicting the PPV could substantially increase computational expenses, especially due to the extensive preprocessing of data and fine-tuning of the model. Balancing computational efficiency with predictive accuracy is crucial in selecting the optimal algorithm for our PPV prediction task, ensuring timely insights into potential blast-induced ground vibrations while maintaining computational feasibility. The comparison of computational cost of this study both for training, testing and validation have summarised in Table 12. Based on Table 12, MD29 shows the highest value of comparison of computational cost such as 0.7243 in training, 0.0180 in testing, and 0.0191 in validation.

Figure 17 shows radar charts that show two mathematical measures used to rate how well training, testing, and validation sets work when using various optimization models[48]. To make it easier to compare the models, a thorough scoring method was employed. Using this method, many success indicators are put together and given a rank number based on how well they work. In our study, we calculate the final score for each model by summing up their individual ranks. The model with the highest total score is considered the best performing one.

Conclusion and summary

A precise and accurate assessment of ground vibration in the mining project is essential to mining engineering. Many researchers developed, trained, tested, and analysed machines, advanced machine, deep, and hybrid learning models in assessing ground vibration. This investigation utilized the conventional and optimized RVM models for the first time in ground vibration prediction. Thus, this work compares 33 RVM models (6 SRVM + 6 SRVM_GA + 6 SRVM_PSO, 5 DRVM, 5 DRVM_GA, 5 DRVM_PSO) to find the optimal performance model. The following conclusions have been mapped from the outcomes of the several analyses.

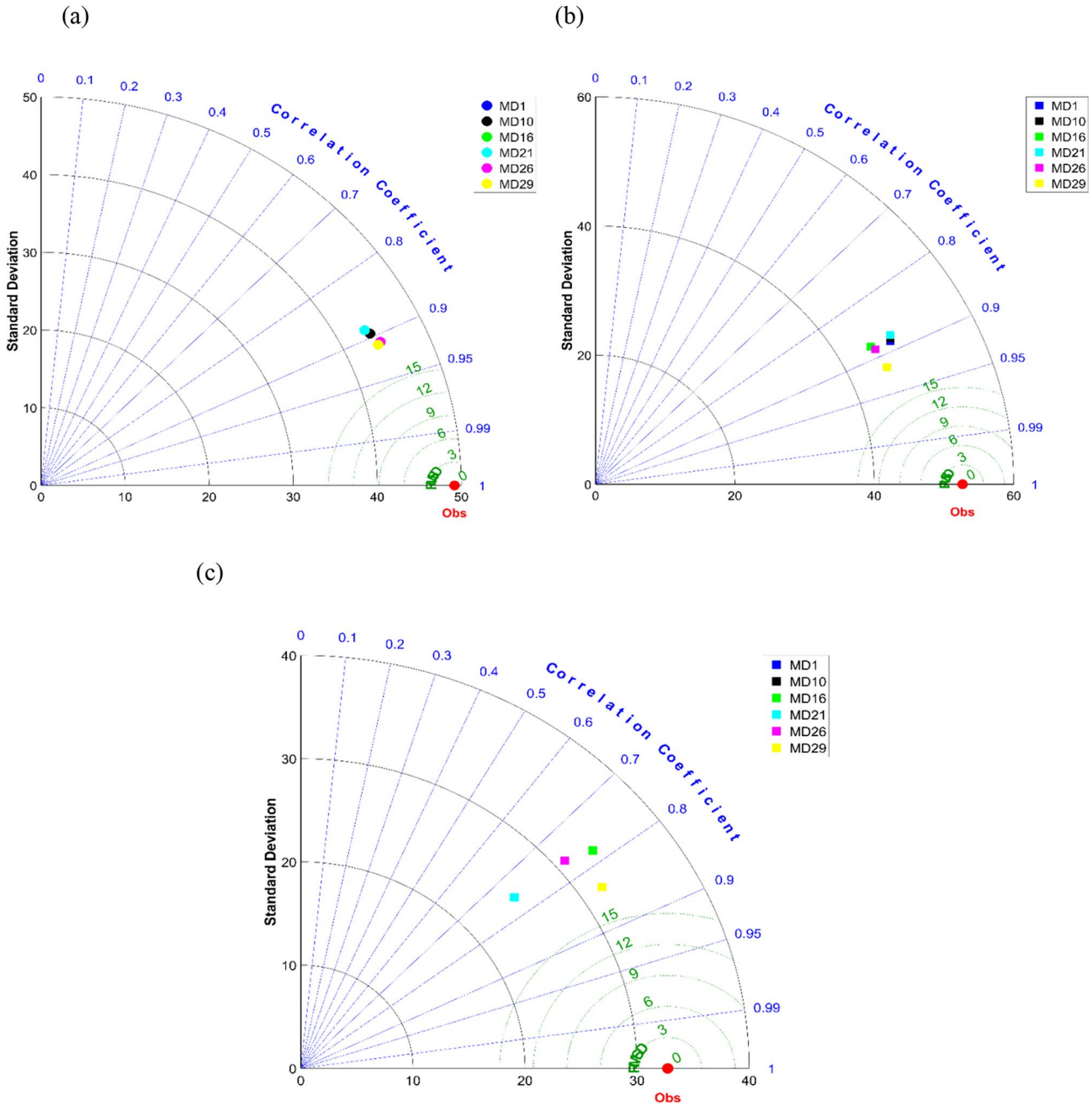

Fig. 15. Illustration of Taylor plots for (**a**) training, (**b**) testing, and (**c**) validation phase.

- Capabilities of RVM models: The performance evaluation of each RVM model demonstrates each model achieved a performance of more than 0.85 in the testing phase, presenting a good agreement between actual and predicted ground vibrations.
- Impact of Dual Kernel: The comparison of conventional SRVM and DRVM models reveals that implementing the secondary kernel function enhances the accuracy and performance of the single kernel based RVM models. Also, dual-kernel RVM models achieve higher computational costs than single-kernel SRVM models.
- Effect of Optimization Algorithm: The genetic and particle swarm algorithms optimized each SRVM and DRVM model in this work. The analysis of performance reveals that the genetic and particle swarm algorithms did not improve the performance of SRVM models. Conversely, a significant performance improvement has been observed for DRVM models. The comparison of SRVM_GA, SRVM_PSO, DRVM_GA, and DRVM_PSO revealed that GA and PSO-optimized DRVM models achieved higher performance than SRVM_GA and SRVM_PSO models.
- Optimal Performance Model : The analysis of performance metrics (RMSE = 21.2999 mm/s, 16.2272 mm/s, R = 0.9175, PI = 1.59, IOA = 0.8239, IOS = 0.2541), score analysis (= 93), REC curve (= 6.85E-03, close to the actual, i.e., 0), curve fitting (= 1.05 close to best fit, i.e., 1), AD test (= 11.607 close to the actual, i.e., 9.790), Wilcoxon test (= 95%), Uncertainty analysis (WCB = 0.0134), and computational cost (= 0.0180) demonstrate

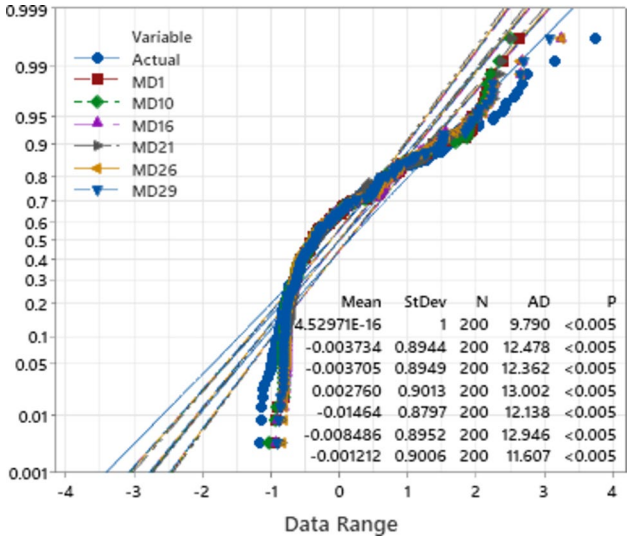

Fig. 16. Depiction of AD test results for models MD1, MD10, MD16, MD21, MD26, and MD29.

Model ID	Num	Median	Confidence levels		Achieved confidence
			LCL	UCL	
Training phase					
Actual	160	0.1859	0.1584	0.2221	95.00%
MD1	160	0.1867	0.1605	0.2219	95.00%
MD10	160	0.1869	0.1608	0.2210	95.00%
MD16	160	0.1836	0.1599	0.2277	95.00%
MD21	160	0.1886	0.1628	0.2218	95.00%
MD26	160	0.1867	0.1621	0.2220	95.00%
MD29	160	0.1838	0.1596	0.2240	95.00%
Testing phase					
Actual	20	0.3140	0.1976	0.4284	95.00%
MD1	20	0.2930	0.1120	0.4435	95.00%
MD10	20	0.2931	0.1126	0.4515	95.00%
MD16	20	0.2998	0.1313	0.4560	95.00%
MD21	20	0.2936	0.1028	0.4831	95.00%
MD26	20	0.3079	0.1365	0.4554	95.00%
MD29	20	0.3085	0.1333	0.4140	95.00%
Validation phase					
Actual	20	0.1992	0.1349	0.2732	95.00%
MD1	20	0.2291	0.1169	0.3587	95.00%
MD10	20	0.2291	0.1169	0.3587	95.00%
MD16	20	0.2291	0.1169	0.3587	95.00%
MD21	20	0.2024	0.1043	0.2892	95.00%
MD26	20	0.2108	0.0982	0.3230	95.00%
MD29	20	0.2143	0.1010	0.2824	95.00%

Table 10. Wilcoxon test for training, testing, and validation phase.

that PSO_DRVM model MD29 outperformed the MD1 (conventional SRVM), MD10 (SRVM_GA), MD16 (SRVM_PSO), MD21 (Conventional DRVM), and MD26 (DRVM_GA) models in the testing phase.

To conclude, the present investigation introduces a particle swarm-optimized Gaussian + exponential kernel-based DRVM model as an optimal performance model for assessing ground vibration in rock blasting. The performance and accuracy of model MD29 demonstrates high capabilities. Therefore, the MD29 model may be implemented to estimate the blasting vibration in mining projects. The current investigation uses 200 data

Model ID	MOE	SD	SE	ME	LB	UB	WCB	Rank
Training phase								
MD1	0.0078	0.0082	0.0006	0.0013	0.0024	0.0132	0.0108	6
MD10	0.0078	0.0082	0.0006	0.0013	0.0031	0.0124	0.0092	5
MD16	0.0073	0.0075	0.0006	0.0012	0.0049	0.0096	0.0047	2
MD21	0.0077	0.0088	0.0007	0.0014	0.0074	0.0080	0.0006	4
MD26	0.0074	0.0075	0.0006	0.0012	0.0057	0.0091	0.0034	3
MD29	0.0072	0.0075	0.0006	0.0012	0.0053	0.0091	0.0038	1
Testing phase								
MD1	0.0091	0.0097	0.0022	0.0043	0.0030	0.0213	0.0182	2
MD10	0.0093	0.0099	0.0022	0.0043	0.0032	0.0217	0.0185	3
MD16	0.0096	0.0091	0.0020	0.0040	0.0027	0.0165	0.0137	6
MD21	0.0095	0.0098	0.0022	0.0043	0.0001	0.0190	0.0189	5
MD26	0.0094	0.0086	0.0019	0.0038	0.0046	0.0141	0.0095	4
MD29	0.0083	0.0074	0.0017	0.0032	0.0016	0.0150	0.0134	1
Validation phase								
MD1	0.0089	0.0079	0.0018	0.0035	0.0007	0.0185	0.0177	6
MD10	0.0089	0.0079	0.0018	0.0035	0.0007	0.0185	0.0177	5
MD16	0.0089	0.0079	0.0018	0.0035	0.0007	0.0185	0.0177	4
MD21	0.0076	0.0082	0.0018	0.0036	0.0016	0.0136	0.0120	2
MD26	0.0081	0.0082	0.0018	0.0036	0.0022	0.0184	0.0162	3
MD29	0.0068	0.0069	0.0015	0.0030	0.0041	0.0177	0.0136	1

Table 11. Results obtained from the uncertainty analysis (UA).

Model	Train	Test	Valid
MD1	0.5342	0.012	0.0141
MD10	0.4892	0.0031	0.0097
MD16	0.1982	0.0016	0.0095
MD21	0.6388	0.0150	0.0168
MD26	0.2491	0.0018	0.0118
MD29	**0.7243**	**0.0180**	**0.0191**

Table 12. Comparison of computational cost. Significant values are in bold.

points, which is a research limitation. The overfitting of the soft computing models may be examined using more field databases. In addition, this investigation may be extended by implementing metaheuristic algorithms, i.e., evolutionary, physical, nature, swarm-based, and biological algorithms. As per the authors' knowledge, the present work implements and compares the single kernel-based SRVM, dual kernel-based DRVM, SRVM_GA, SRVM_PSO, DRVM_GA, and DRVM_PSO models in assessing the ground vibrations for the first time. This research will help mining engineers and designers select the best kernel function and its hyperparameters in estimating ground vibration. Future research directions of this study include applying the model to different geological conditions, rock mass condition and explosive property and comparing its performance against other state-of-the-art predictive models. Additionally, investigating the impact of varying blasting parameters and environmental conditions on ground vibration predictions will provide more comprehensive insights.

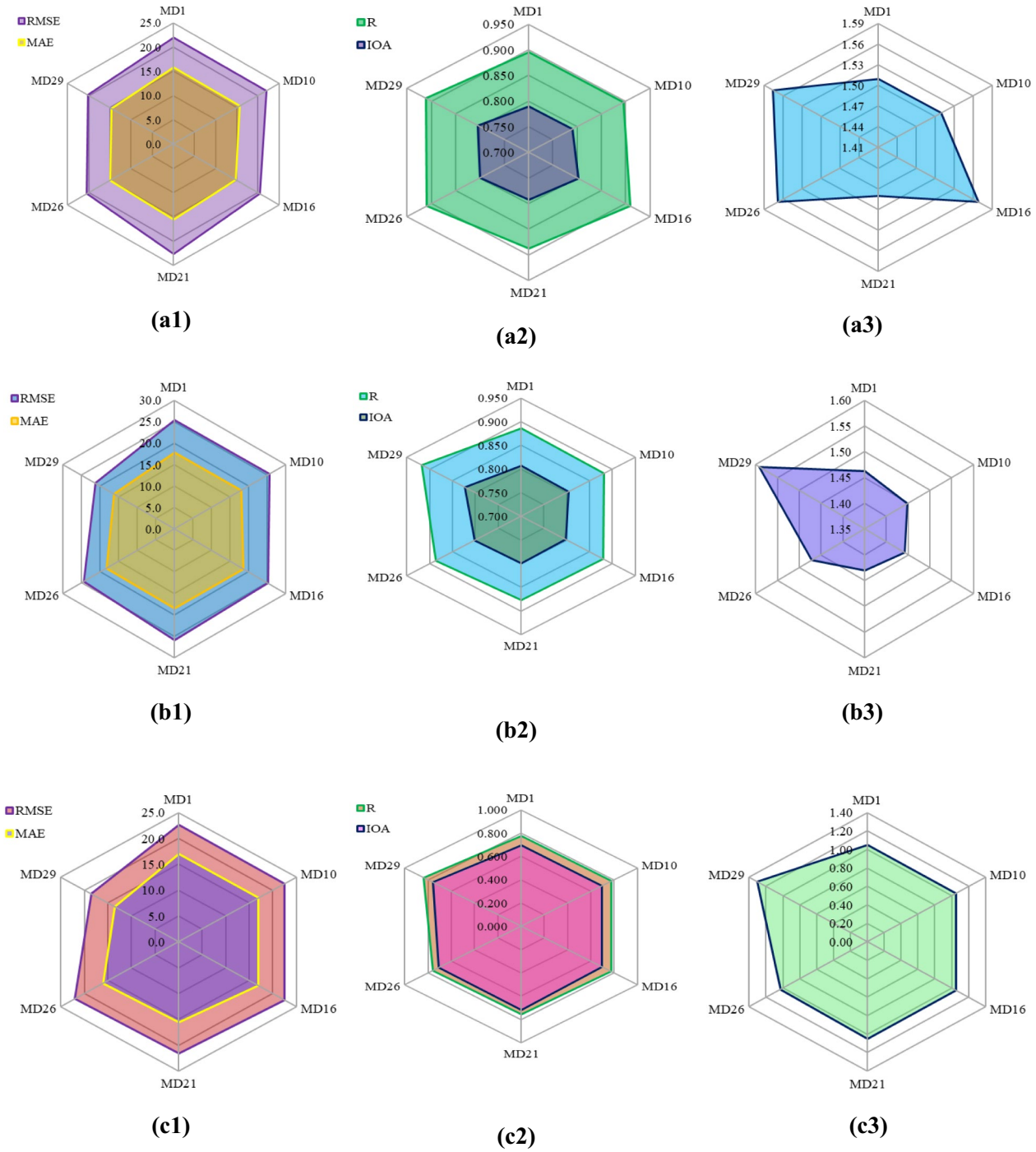

Fig. 17. Illustration of radar plots of RMSE & MAE (**a1**, **b1**, **c1**), R & IOA (**a2**, **b2**, **c2**), and PI (**a3**, **b3**, **c3**) in the prediction of ground vibration during (**a**) training, (**b**) testing, (**c**) validation.

Data availability

All data generated or analysed during this study are included in this article.

Received: 11 June 2024; Accepted: 22 August 2024
Published online: 28 August 2024

References

1. B. O. Taiwo *et al.* Assessment of charge initiation techniques effect on blast fragmentation and environmental safety: An application of WipFrag software. 1–17 (2023).
2. Taiwo, B. O. *et al.* Artificial neural network modeling as an approach to limestone blast production rate prediction: A comparison of PI-BANN and MVR models. *J. Min. Environ.* **14**(2), 375–388. https://doi.org/10.22044/jme.2023.12489.2266 (2023).
3. Y. Fissha, H. Ikeda, H. Toriya, N. Owada, T. Adachi, & Y. Kawamura. Evaluation and prediction of blast-induced ground vibrations: A Gaussian Process Regression (GPR) Approach. 659–682 (2023).
4. Zhou, J., Li, C., Koopialipoor, M., Armaghani, D. J. & Pham, B. T. Development of a new methodology for estimating the amount of PPV in surface mines based on prediction and probabilistic models (GEP). *Int. J. Mining Reclam. Environ.* **35**(1), 48–68. https://doi.org/10.1080/17480930.2020.1734151 (2021).
5. H. Zhang, J. Zhou, D. J. Armaghani, M. M. Tahir, & B. T. Pham. Applied sciences A combination of feature selection and random forest techniques to solve a problem related to. *Appl. Sci.* (2020).
6. Choudhary, B. S. & Agrawal, A. Minimization of blast-induced hazards and efficient utilization of blast energy by implementing a novel stemming plug system for eco-friendly blasting in open pit mines. *Nat. Resour. Res.* **31**(6), 3393–3410. https://doi.org/10.1007/s11053-022-10126-8 (2022).
7. Olamide Taiwo, B. Improvement of small-scale dolomite blasting productivity: Comparison of existing empirical models with image analysis software and artificial neural network models. *J. Min. Environ.* **13**(3), 627–641. https://doi.org/10.22044/jme.2022.11771.2169 (2022).
8. Fissha, Y., Ikeda, H., Toriya, H., Adachi, T. & Kawamura, Y. Application of Bayesian Neural Network (BNN) for the prediction of blast-induced ground vibration. *Appl. Sci.* https://doi.org/10.3390/app13053128 (2023).
9. Zhou, J., Zhang, Y. & Qiu, Y. *State-of-the-Art Review of Machine Learning and Optimization Algorithms Applications in Environmental Effects of Blasting* (Springer Netherlands., 2024). https://doi.org/10.1007/s10462-023-10636-8.
10. Hosseini, S. *et al.* Assessment of the ground vibration during blasting in mining projects using different computational approaches Cosine amplitude method. *Sci. Rep.* https://doi.org/10.1038/s41598-023-46064-5 (2023).
11. Lawal, A. I., Kwon, S., Hammed, O. S. & Idris, M. A. Blast-induced ground vibration prediction in granite quarries: An application of gene expression programming, ANFIS, and sine cosine algorithm optimized International Journal of Mining Science and Technology Blast-induced ground vibration prediction in. *Int. J. Min. Sci. Technol.* https://doi.org/10.1016/j.ijmst.2021.01.007 (2021).
12. Chen, W., Hasanipanah, M., Nikafshan Rad, H., Jahed Armaghani, D. & Tahir, M. M. A new design of evolutionary hybrid optimization of SVR model in predicting the blast-induced ground vibration. *Eng. Comput.* **37**(2), 1455–1471. https://doi.org/10.1007/s00366-019-00895-x (2021).
13. S. Alzabeebee, M. Jamei, M. Hasanipanah, & H. B. Amnieh. Development of a new explicit soft computing model to predict the blast-induced ground vibration. (2022), https://doi.org/10.12989/gae.2022.30.6.551.
14. Erten, O., Konak, G., Kizil, M. S., Onur, A. H. & Karakus, D. Analysis of quarry-blast-induced ground vibrations to mitigate their adverse effects on nearby structures. *Int. J. Min. Miner. Eng.* **1**(4), 313–326. https://doi.org/10.1504/IJMME.2009.029317 (2009).
15. Khandelwal, M. & Singh, T. N. Prediction of blast-induced ground vibration using artificial neural network. *Int. J. Rock Mech. Min. Sci.* **46**(7), 1214–1222. https://doi.org/10.1016/j.ijrmms.2009.03.004 (2009).
16. Zhang, Y., He, H., Khandelwal, M., Du, K. & Zhou, J. Knowledge mapping of research progress in blast-induced ground vibration from 1990 to 2022 using CiteSpace-based scientometric analysis. *Environ. Sci. Pollut. Res.* **30**(47), 103534–103555. https://doi.org/10.1007/s11356-023-29712-1 (2023).
17. Ragam, P. & Nimaje, D. S. Assessment of blast-induced ground vibration using different predictor approaches—A comparison. *Chem. Eng. Trans.* **66**, 487–492. https://doi.org/10.3303/CET1866082 (2018).
18. Alipour, A., Mokhtarian, M. & Sharif, J. A. Artificial neural network or empirical criteria? A comparative approach in evaluating maximum charge per delay in surface mining—Sungun copper mine. *J. Geol. Soc. India* **79**(6), 652–658. https://doi.org/10.1007/s12594-012-0102-3 (2012).
19. Taheri, K., Hasanipanah, M., Golzar, S. B. & Majid, M. Z. A. A hybrid artificial bee colony algorithm-artificial neural network for forecasting the blast-produced ground vibration. *Eng. Comput.* **33**(3), 689–700. https://doi.org/10.1007/s00366-016-0497-3 (2017).
20. Nguyen, H., Bui, X.-N. & Topal, E. Reliability and availability artificial intelligence models for predicting blast-induced ground vibration intensity in open-pit mines to ensure the safety of the surroundings. *Reliab. Eng. Syst. Saf.* **231**, 109032 (2023).
21. Zhang, H. *et al.* A combination of feature selection and random forest techniques to solve a problem related to blast-induced ground vibration. *Appl. Sci.* https://doi.org/10.3390/app10030869 (2020).
22. Zhou, J., Asteris, P. G., Armaghani, D. J. & Pham, B. T. Prediction of ground vibration induced by blasting operations through the use of the Bayesian Network and random forest models. *Soil Dyn. Earthq. Eng.* https://doi.org/10.1016/j.soildyn.2020.106390 (2020).
23. Huang, J., Koopialipoor, M. & Armaghani, D. J. A combination of fuzzy Delphi method and hybrid ANN-based systems to forecast ground vibration resulting from blasting. *Sci. Rep.* **10**(1), 1–21 (2020).
24. J. Zhou, C. Li, M. Koopialipoor, D. J. Armaghani, B. T. Pham. (2020) Development of a new methodology for estimating the amount of PPV in surface mines based on prediction and probabilistic models (GEP-MC). *Int. J. Mining, Reclam. Environ*. https://doi.org/10.1080/17480930.2020.1734151.
25. Nguyen, H., Bui, X.-N., Tran, Q.-H. & Mai, N.-L. A new soft computing model for estimating and controlling blast-produced ground vibration based on hierarchical K-means clustering and cubist algorithms. *Appl. Soft Comput.* **77**, 376–386 (2019).
26. Nguyen, H., Choi, Y., Bui, X. N. & Nguyen-Thoi, T. Predicting blast-induced ground vibration in open-pit mines using vibration sensors and support vector regression-based optimization algorithms. *Sensors (Switzerland).* https://doi.org/10.3390/s20010132 (2020).
27. Armaghani, D. J., Hasanipanah, M., Amnieh, H. B. & Mohamad, E. T. Feasibility of ICA in approximating ground vibration resulting from mine blasting. *Neural Comput. Appl.* **29**(9), 457–465 (2018).
28. Hasanipanah, M., Faradonbeh, R. S., Amnieh, H. B., Armaghani, D. J. & Monjezi, M. Forecasting blast-induced ground vibration developing a CART model. *Eng. Comput.* https://doi.org/10.1007/s00366-016-0475-9 (2017).
29. Ghoraba, S., Monjezi, M., Talebi, N., Armaghani, D. J. & Moghaddam, M. R. Estimation of ground vibration produced by blasting operations through intelligent and empirical models. *Environ. Earth Sci.* https://doi.org/10.1007/s12665-016-5961-2 (2016).
30. Shirani Faradonbeh, R. *et al.* Prediction of ground vibration due to quarry blasting based on gene expression programming: A new model for peak particle velocity prediction. *Int. J. Environ. Sci. Technol.* https://doi.org/10.1007/s13762-016-0979-2 (2016).
31. Hajihassani, M., Armaghani, D. J., Marto, A. & Mohamad, E. T. Ground vibration prediction in quarry blasting through an artificial neural network optimized by imperialist competitive algorithm. *Bull. Eng. Geol. Environ.* **74**(3), 873–886 (2015).
32. M. Hajihassani, D. Jahed, & A. Masoud. Blast-induced air and ground vibration prediction: A particle swarm optimization-based artificial neural network approach. (2015). https://doi.org/10.1007/s12665-015-4274-1.
33. Hasanipanah, M., Monjezi, M., Shahnazar, A., Jahed Armaghani, D. & Farazmand, A. Feasibility of indirect determination of blast induced ground vibration based on support vector machine. *Meas. J. Int. Meas. Confed.* https://doi.org/10.1016/j.measurement.2015.07.019 (2015).

34. Armaghani, D. J., Momeni, E., Abad, S. V. A. N. K. & Khandelwal, M. Feasibility of ANFIS model for prediction of ground vibrations resulting from quarry blasting. *Environ. Earth Sci.* https://doi.org/10.1007/s12665-015-4305-y (2015).
35. Armaghani, D. J., Hajihassani, M., Mohamad, E. T., Marto, A. & Noorani, S. A. Blasting-induced flyrock and ground vibration prediction through an expert artificial neural network based on particle swarm optimization. *Arab. J. Geosci.* 7(12), 5383–5396 (2014).
36. Mohamadnejad, M., Gholami, R. & Ataei, M. Comparison of intelligence science techniques and empirical methods for prediction of blasting vibrations. *Tunn. Undergr. Sp. Technol.* **28**, 238–244 (2012).
37. Monjezi, M., Hasanipanah, M. & Khandelwal, M. Evaluation and prediction of blast-induced ground vibration at Shur River Dam, Iran, by artificial neural network. *Neural Comput. Appl.* **22**(7–8), 1637–1643. https://doi.org/10.1007/s00521-012-0856-y (2013).
38. Mohamed, M. T. Performance of fuzzy logic and artificial neural network in prediction of ground and air vibrations. *JES. J. Eng. Sci.* **39**(2), 425–440 (2011).
39. A. Fi & C. Kuzu. Prediction of environmental impacts of quarry blasting operation using fuzzy logic. 461–470 (2011). https://doi.org/10.1007/s10661-010-1470-z.
40. Iphar, M., Yavuz, M. & Ak, H. Prediction of ground vibrations resulting from the blasting operations in an open-pit mine by adaptive neuro-fuzzy inference system. *Environ. Geol.* https://doi.org/10.1007/s00254-007-1143-6 (2008).
41. Hammed, O. S. *et al.* Peak particle velocity data acquisition for monitoring blast induced earthquakes in quarry sites. *Data Br.* **19**, 398–408. https://doi.org/10.1016/j.dib.2018.04.103 (2022).
42. Bahmed, I. T., Khatti, J. & Grover, K. S. Hybrid soft computing models for predicting unconfined compressive strength of lime stabilized soil using strength property of virgin cohesive soil. *Bull. Eng. Geol. Environ.* https://doi.org/10.1007/s10064-023-03537-1 (2024).
43. Khatti, J., Grover, K. S., Kim, H. J., Mawuntu, K. B. A. & Park, T. W. Prediction of ultimate bearing capacity of shallow foundations on cohesionless soil using hybrid LSTM and RVM approaches: An extended investigation of multicollinearity. *Comput. Geotech.* **165**, 105912. https://doi.org/10.1016/j.compgeo.2023.105912 (2024).
44. J. Qui. Learning with uncertainty—Gaussian processes and relevance vector machines. (2004).
45. Ghorbani, B., Arulrajah, A., Narsilio, G., Horpibulsuk, S. & Win, M. ScienceDirect Development of genetic-based models for predicting the resilient modulus of cohesive pavement subgrade soils. *Soils Found.* **60**(2), 398–412. https://doi.org/10.1016/j.sandf.2020.02.010 (2020).
46. J. Khatti, H. Samadi, & K. S. Grover. in *Estimation of Settlement of Pile Group in Clay Using Soft Computing Techniques*, no. 0123456789. (Springer International Publishing, 2023). https://doi.org/10.1007/s10706-023-02643-x.
47. Bardhan, A., Samui, P., Ghosh, K., Gandomi, A. H. & Bhattacharyya, S. ELM-based adaptive neuro swarm intelligence techniques for predicting the California bearing ratio of soils in soaked conditions. *Appl. Soft Comput.* **110**, 107595. https://doi.org/10.1016/j.asoc.2021.107595 (2021).
48. Xi, B., Li, E., Fissha, Y., Zhou, J. & Segarra, P. LGBM-based modeling scenarios to compressive strength of recycled aggregate concrete with SHAP analysis. *Mech. Adv. Mater. Struct.* https://doi.org/10.1080/15376494.2023.2224782 (2023).

Author contributions

Y.F, and J.K: Conceptualization, Methodology, Investigation, Software, Writing – original draft, Application of AI models, Relevance vector machine model development, Statistical analysis, Detailing, and Overall analysis. H.I, K.S.G, and H.T.: Conceptualization, Resources, Supervision, Testing. Y.F and J.K.: Conceptualization, Writing – original draft, Methodology, Software, Investigation, Resources, Validation, Formal analysis. Y.F, N.O. and J.K.: Investigation, Formal analysis, Validation, Software, Writing – review & editing. H.I, K.S.G, T.A, and H.T.: Visualization, Validation, Project administration, acquired the funding for this research.: Investigation, Formal analysis, Validation, Software, Writing – review & editing. H.T. T.A., and Y. K.: Visualization, Project administration, Software, Formal analysis, Validation, Writing – review & editing.

Funding

Yewuhalashet Fissha want to acknowledge the funding supported by Akita University Fellowship Program.

Competing interests

The authors declare no competing interests.

Additional information

Correspondence and requests for materials should be addressed to Y.F. or J.K.

Reprints and permissions information is available at www.nature.com/reprints.

Publisher's note Springer Nature remains neutral with regard to jurisdictional claims in published maps and institutional affiliations.